NASA TECHNICAL NOTE

NASA TN D-2813

OBSERVATIONS OF INTERNAL OXIDATION IN SIX NICKEL-BASE ALLOY SYSTEMS

by James S. Wolf, John W. Weeton, and John C. Freche

Lewis Research Center

Cleveland, Ohio

NATIONAL AERONAUTICS AND SPACE ADMINISTRATION • WASHINGTON, D. C. • MAY 1965

NASA TN D-2813

OBSERVATIONS OF INTERNAL OXIDATION IN SIX NICKEL-BASE ALLOY SYSTEMS

By James S. Wolf, John W. Weeton, and John C. Freche

Lewis Research Center
Cleveland, Ohio

NATIONAL AERONAUTICS AND SPACE ADMINISTRATION

For sale by the Clearinghouse for Federal Scientific and Technical Information
Springfield, Virginia 22151 - Price $3.00

OBSERVATIONS OF INTERNAL OXIDATION IN SIX NICKEL-BASE ALLOY SYSTEMS

by James S. Wolf, John W. Weeton, and John C. Freche

Lewis Research Center

SUMMARY

23169

An internal oxidation investigation was conducted with a series of solid solution nickel-base binary alloys (nickel (Ni) with aluminum (Al), magnesium (Mg), silicon (Si), titanium (Ti), chromium (Cr), and manganese (Mn)). These systems were studied to determine their potentials as dispersion-strengthened materials and to gain some additional insight into methods whereby the internal oxidation approach may be utilized to create improved aerospace materials. The alloys were air oxidized for 200 hours at 1200°, 1500°, and 1800° F and were then subsequently stability annealed in vacuum for 24 hours at 2000° F.

The major results were as follows:

(1) Subscale penetration increased with decreasing solute concentration and increasing oxidation temperature. Penetrations as great as approximately 850 microns as a result of oxidation alone were observed.

(2) External scales decomposed during the stability anneal and provided a source of oxygen that caused further oxide penetration into the specimens; this was observed especially in those cases of prior low-temperature oxidation which produced no observable subscale.

(3) The stability anneals, subsequent to the higher temperature oxidation treatments, promoted only minor changes in the size and shape of existing internal oxides.

(4) The subscale morphology differed among the different systems and included small, closely spaced particles (Ni-Mg), highly oriented acicular particles (Ni-Al), and large, widely spaced angular oxides (Ni-Cr and Ni-Mn).

(5) Based on optical microscopy, two alloys (Ni - 1.32 atomic percent Mg and Ni - 0.98 atomic percent Si) appeared to be particularly amenable for application as dispersion-strengthened materials. The subscale oxides developed in these alloys had characteristics analogous to those found in sintered aluminum powder. The oxide particle diameters were 0.11 and 0.4 micron, respectively; the interparticle spacings were 0.73 and 6 microns, respectively.

Author

INTRODUCTION

Dispersoids have been produced in numerous alloys by the processes of internal oxidation. Subsurface oxides in the form of small dispersed spheroids or needles may, in many alloys, be formed by exposing the alloy to an oxygen-bearing atmosphere at elevated temperatures. Basically, the internal oxidation process occurs by selective oxidation of one constituent of the alloy. A comprehensive discussion of the mechanisms involved has been presented in references 1 to 3. Although the abilities of internally formed oxides to retard recrystallization and to strengthen alloys were recognized in the 1940's (refs. 1 and 4), it was not until later that the process was given serious consideration as a method of providing structurally sound dispersion-strengthened alloys. Actually, it was not until after the full potentialities of dispersion-strengthened products were made graphically evident by R. Irmann (ref. 5) that serious attempts were made to produce dispersion-strengthened products by internal oxidation methods. The SAP (sintered aluminum powder) products produced by Irmann were made by another process, namely, from the extrusion of cold-pressed and sintered aluminum powders. Thin films of aluminum oxide that formed naturally on the surfaces of these powders were broken up and the fragments dispersed by the extrusion process. The long-time high-temperature stability of these products was outstanding.

Numerous investigations have been conducted to study internal oxidation of various materials in an attempt to produce dispersion-strengthened products (refs. 6 to 11). Some of the strongest SAP-type materials that have been made utilize internal oxidation methods. Some have exhibited excellent high-temperature tensile and creep-rupture strength; in fact, some have creep strength that is analogous to the strength achieved in aluminum SAP (ref. 6).

There are several inherent and potential problems associated with producing stable, high-strength, high-melting-point, dispersion-strengthened products by internal oxidation. The size of the internal oxide particles may vary significantly as the depth of subscale penetration increases; for example, Bonis and Grant (ref. 12) have observed particle size variations of over 300 percent. Other investigators have shown that the particle sizes of the oxides at grain boundaries are much larger than particles within grains (refs. 7 and 13 to 17), while Rhines (ref. 14) has noted that subscale penetrations may proceed preferentially at grain boundaries. Finally, surface oxides consisting largely of the solvent metal oxide would have to be reduced or eliminated to permit fabrication of satisfactory internally oxidized products. All of these phenomena could lead to undesirable banded, segregated, or agglomerated oxides after subsequent mechanical processing, which may be employed in the production of dispersion-strengthened products.

Since the strength and stability of dispersion-strengthened products, including those made by internal oxidation, depend to a large extent on the uniformity of the microstructure, it was felt that additional information about the process of internal oxidation per se was desirable. Therefore this exploratory investigation was conducted to study internal oxidation of several nickel-base binary alloys to determine the effects of oxidation temperature and solute concentration on the depth of oxide penetration and subscale morphology. In addition, the investigation was conducted to study the thermal stability of

internal oxide formations under a high-temperature anneal. It was believed that such studies would also provide additional knowledge and a better understanding of the problems associated with the development of alloys or composites made from materials containing internal oxides. Such alloys would have considerable current significance in aerospace applications where their inherent long-time high-temperature stability and strength could be used to full advantage. Specific applications could include turbine engine components for use in advance aircraft such as the supersonic transport and advanced space-power systems.

Oxidation tests were conducted in air with cast specimens of each alloy system (nickel (Ni) with aluminum (Al), magnesium (Mg), silicon (Si), titanium (Ti), chromium (Cr), and manganese (Mn)) oxidized in air for 200 hours at temperatures of 1200°, 1500°, and 1800° F. The stability of the subsurface oxides formed was explored by employing subsequent stability heat treatments for 24 hours at 2000° F. Studies were made of subscale penetrations, hardness, and morphology.

EXPERIMENTAL PROCEDURE

Preparation of Specimens for Oxidation

Casting procedure. - Master melts were made of binary nickel-base alloys of aluminum, magnesium, silicon, titanium, chromium, or manganese. These alloys were prepared by induction melting under 1 atmosphere of argon in order to minimize oxidation of the melt constituents. The percent purities of the metals used, as determined by the suppliers, were as follows: nickel, 99.95; aluminum, 99+; magnesium, 99.5; silicon, 98+; titanium, 99.2; chromium, 99.3; and manganese, 99+. Charges were melted in zircon crucibles and held in the molten state for 3 to 5 minutes prior to pouring in order to insure homogeneity of the master melt. Melts were poured (under argon) into cold copper molds. Test alloys of the desired compositions were subsequently produced by remelting the master melts together with electrolytic nickel under conditions identical to those described previously. The amount of zirconium assimilated by the test alloys during the melting processes was not detectable spectrographically; however, chemical analysis indicated silicon "pickup" ranged from 0.007 to 0.05 percent.

Chemical analyses. - Chemical analyses were made of each of the master alloy castings in order to determine the amount of electrolytic nickel required for the remelt process. A second chemical analysis was made of each test alloy to determine the final composition. Oil-free turnings were removed from the central sections of the castings to provide material for these analyses. The alloy compositions considered for each of the binary systems under investigation are shown in table I (p. 4). All compositions were within the solid solution regions of their respective nickel-additive binary systems.

Specimen fabrication. - Cylindrical test alloy castings were cut normal to their longitudinal axes to provide 1/2-inch-diameter specimens approximately 3/16 of an inch in thickness. Each specimen was polished on both flat faces with metallographic polishing papers; the final paper was 600 grit.

TABLE I. - ALLOY COMPOSITIONS INVESTIGATED

Binary system	Solute, atomic percent	Binary system	Solute, atomic percent
Ni-Al	0.48 Al 1.66 3.52 9.01	Ni-Ti	0.086 Ti .98 3.01 10.8
Ni-Mg	0.27 Mg .43 1.32	Ni-Cr	0.088 Cr .76 3.69 9.13
Ni-Si	0.073 Si .98 3.00 8.77	Ni-Mn	0.075 Mn .75 2.94 8.93

Oxidation Treatments

Initial oxidation. - Polished specimens were oxidized in firebrick furnaces heated by globar-type elements. A stagnant air oxidizing atmosphere was employed. One sample of each alloy was oxidized at each of the following temperatures: 1200° F, 1500° F, and 1800° F for 200 hours. The specimens were placed in Alundum furnace boats in such a way that both of their flat surfaces were completely exposed to the oxidizing atmosphere. Oxidation temperatures cited were measured by means of a thermocouple located immediately above the furnace boat and were maintained within ±5° F. All the compositions of a given alloy system (maximum of four samples) were oxidized simultaneously to eliminate the possibility of solute contamination of one system by another. Upon removal from the furnace, specimens were air cooled.

Stability heat treatment. - After initial oxidation treatments, the disk-shaped specimens were cut diametrically into two sections. One of the sections was prepared for metallographic examination and the other was heat treated in order to determine the high-temperature stability of the subsurface oxides formed during initial oxidation. The latter specimens were placed in a resistance-heated ceramic-lined vacuum furnace for 24 hours at a temperature of 2000° F. A pressure of 10^{-5} to 10^{-6} atmosphere of air was maintained throughout this process. Specimens were air cooled upon completion of the stability treatment.

Microhardness Tests

Specimens used in microhardness determinations were mounted, polished, and etched for 15 seconds with a nickel etch (92 ml HCl, 3 ml HNO_3, and 5 ml H_2SO_4). A microhardness tester equipped with a standard 136° diamond penetrator loaded to 1 kilogram was employed to determine the hardness values for each specimen at both the central portions of the subscale and in the zone unaffected by subscale formation. The average of 10 measurements, taken in each zone of each specimen, was determined. In a few cases, where the subscale penetration was too small to accommodate the indentation made with a 1-kilogram load, a 50-gram load was employed. In these instances the average hardness numbers obtained were converted to those of an equivalent 1-kilogram load by the method of linear proportions. Alloys that had been oxidized at 1800° F were hardness tested before and after their stability heat treatments; those oxidized at lower temperatures were not hardness tested because of the relatively small subscale penetrations developed.

Metallographic Studies

Specimens used in metallographic examinations were mounted in Bakelite, polished in a manner which preserved one edge of the specimen, and etched with modified Marble's reagent (2.5 g $CuCl_2$ dissolved in 125 ml H_2O, 97 ml HCl, and 3 ml HNO_3). Photomicrographs of the preserved edges of as-oxidized and stability heat-treated specimens were taken and the penetration and morphological characteristics of the subscales formed in each of the alloys considered were determined. The values of subscale penetrations measured represent the thickness of that zone contained between the external oxide-subscale interface and the subscale-alloy interface. Penetration measurements were taken directly from photomicrographs of various known magnifications and converted to actual depth dimensions. Two alloys (Ni - 1.32 atomic percent Mg and Ni - 0.98 atomic percent Si) that exhibited larger numbers of finely dispersed subscale oxides were selected for further study by electron microscope techniques. Specimens of these alloys were vibratory polished, etched with modified Marble's reagent, shadowed with chromium, and replicated with silicon monoxide. Electron photomicrographs of the replicas were used for a determination of the volume fraction oxide, the average particle size, and the distribution of particle sizes, as well as the interparticle spacing of the subscale oxides formed in these alloys.

RESULTS

Subscale Penetration Studies

The depth of subscale penetration (based on metallographic investigation) for the various alloys in the as-oxidized and the as-oxidized plus stability heat-treated conditions is shown as a function of composition and oxidizing temperature in figures 1(a) to 1(f). In general, for both of these conditions, the amount of subscale formed (i.e., depth of penetration) was observed to decrease as the solute concentration was increased.

The effect of oxidizing temperature on the penetration behavior is also shown in figure 1. It is evident that the temperature of oxidation greatly affected the degree of penetration; larger penetrations are associated with higher temperatures of oxidation for all of the systems investigated. Furthermore, this effect is more pronounced in alloys of low solute concentrations. Summary plots of the curves of the 1800° F as-oxidized data are presented in figure 2. Subscale penetrations up to approximately 850 microns were observed to result from the oxidation treatment alone.

The stability heat treatment produced an increased depth of subscale penetration in each of the alloy systems considered regardless of the temperature of the initial oxidation treatment.

It should be noted that the stability anneal, although performed in a vacuum, was made with specimens having a considerable external scale produced originally by the initial internal oxidation. In a sense, the high temperature so called "stability anneal" was an additional internal oxidation treatment

since the surface scale as well as the residual air in the vacuum furnace undoubtedly acted as sources of oxygen. This increase was more noticeable in those alloys that contained a low concentration of solute. Also, specimens that were initially oxidized at 1200° or 1500° F were affected by the stability treatment to a greater degree than those initially internally oxidized at 1800° F. Curves for the Ni-Al system (fig. 1(a)) are representative of the general response of all the systems studied to the stability heat treatment.

Hardness Studies

The microhardnesses of the subscale and the unoxidized zones of binary alloy specimens oxidized at 1800° F, both before and after the stability heat treatment, are shown in figures 3(a) to 3(f) as functions of solute concentration. Hardness measurements for the lower temperature oxidation conditions were not attempted because of the small subscale penetrations obtained. Values of hardness ranged from approximately 70 to 300 diamond pyramid hardness in the subscale zones and from approximately 70 to 150 diamond pyramid hardness in the central zones. In general, the hardness of the subscale zone exceeded that of the unoxidized zone. An initial increase in subscale hardness followed by a decrease at higher solute concentrations was observed in the Ni-Si, Ni-Cr, and Ni-Mn systems. For these systems, the hardness of the subscale zone was lower than that of the central (unoxidized) zone at higher solute concentrations. The stability heat treatment generally reduced the hardness of both the subscale and the unoxidized regions of the alloys investigated. This reduction in subscale hardness was particularly noticeable at the higher solute concentrations for the Ni-Al, Ni-Ti, and Ni-Mn alloys.

For comparison, a summary plot of the variation of subscale hardness with composition for each binary system in the 1800° F as-oxidized condition is shown in figure 4. Except for the Ni-Si and Ni-Cr systems, a nearly linear increase in hardness with increasing solute concentration was noted. The largest increase in hardness, up to approximately 300 diamond pyramid hardness, was obtained with the Ni-Al system. The Ni-Mn alloy system exhibited one of the smallest increases in hardness, up to approximately 110 diamond pyramid hardness, with increasing solute concentration.

Morphology of Internal Oxides

Each alloy system was investigated metallographically in order to determine the effects of alloy composition, oxidizing temperature, and stability heat treatment on the morphological characteristics of the subscales formed by oxidation at 1800° F. Since the degree of subscale formation at the lower oxidizing temperatures (1200° and 1500° F) was limited, metallographic studies of specimens oxidized at these temperatures are presented for only the Ni-Al system. Figures 5 to 10 provide photomicrographs at a magnification of 500 for each of the alloy systems investigated.

As-oxidized. - Figure 5 shows photomicrographs of the as-oxidized Ni-Al alloys. It is evident from examination of the photomicrographs of this figure that temperature has a significant effect on the morphological characteristics

of the subsurface oxides (figs. 5(a) to 5(l)). For a given concentration increase, the depths of penetration of the internal oxides and the oxide particle sizes increased as the oxidizing temperature was increased. The volume fraction of oxides decreased with increasing temperature between 1500° and 1800° F. At 1200° F there was no observable penetration; some penetration of particles (large spheroids) occurred at 1500° F. In one of the figures (fig. 5(f)) there is evidence of preferential penetration of oxides along the grain boundaries. Similar penetrations have been observed in other specimens of Ni-Al internally oxidized at 1500° F (unpublished NASA data). At 1800° F a large volume percent of precipitates was evident. In addition, there was a tendency for the aluminum oxide particles to be acicular after oxidation at 1800° F.

The descriptions of the morphological changes that follow include all of the systems studied for an internal oxidizing temperature of 1800° F. It should again be noted that only one internal oxidation temperature was used for morphological studies of systems other than the Ni-Al system. Metallographic examination showed that significant changes in structure occurred with all of the materials as concentration of the solute elements was varied. There was a tendency to form spheroids at the lowest concentrations of solute in all of the systems. As solute concentration was increased there was a tendency to form acicular structures in the Ni-Al and the Ni-Cr systems. Increases in volume percent of subscale oxides with increasing solute concentrations were generally observed for all the systems, except at the highest solute concentration for the Ni-Cr and the Ni-Si systems. Interparticle spacings (separation between oxides) appeared to decrease with increasing solute concentration except in the case of the Ni-Mn system. In general, the Ni-Cr and Ni-Mn systems exhibited oxide particles that were relatively large compared to the particles present in the other oxidized alloy systems.

As-oxidized plus stability annealed. - The stability treatment, consisting of a 2000° F heat treatment for 24 hours in vacuum, was applied to specimens that had previously been oxidized. Decomposition of the surface scales formed during the oxidizing treatments occurred during the stability annealing treatments. This decomposition of the surface oxides provided a source of oxygen for continued internal oxidation. Furthermore, the vacuum was not sufficiently high to prevent additional oxidation by residual gases from occurring. As a result, the depths of penetration were generally increased during the stability annealing treatment. In some cases there were penetrations where none had previously existed. With the Ni-Al, Ni-Mg, Ni-Si, and Ni-Cr alloys, no gross structural changes were observed in the oxide morphology as a result of the stability annealing. In the case of Ni-Ti and Ni-Mn systems, a major structural change was observed in that there was a tendency for the oxides to agglomerate into spheroids - especially those alloys of higher solute concentration.

Miscellaneous observations. - In the case of the Ni-Al, Ni-Ti, and Ni-Cr systems, the particle sizes of the oxide tended to become larger as the depth of penetration increased. In some systems, such as Ni-Si and Ni-Cr at the highest solute concentrations, the external scales appeared to be so resistant to oxygen penetration that the region adjacent to them did not exhibit significant amounts of subscale formation. In the case of the Ni-Mn specimens, the proportion of large oxides relative to small oxides varied; in some cases, the large oxides were close to the external surface while in others they were at the internal

oxide-unoxidized alloy interface.

It is interesting to note that in the highest silicon-bearing alloy, oxidation appeared to be completely stopped for both the initially oxidized specimens and the stability heat-treated specimens (fig. 7(d)). High solute contents in the Ni-Al, Ni-Ti, and Ni-Cr systems also inhibited the production of the internally oxidized zone (figs. 5(d), 8(d), and 9(d)).

DISCUSSION

Applicability of Results to Dispersion Strengthening

Electron micrographic studies. - Two of the alloys appeared to have structures that particularly warranted electron micrographic study; namely, the Ni-Mg alloy with 1.32 atomic percent magnesium (fig. 6(d)) and a Ni-Si alloy with 0.98 percent silicon (fig. 7(e)). The distribution of subscale oxide particle sizes of these alloys is shown in figure 11. The average interparticle spacing measured for the magnesium bearing internally oxidized alloy was 0.73 micron, the average particle size was 0.11 micron, and the volume percent of oxide was 12.2 in the microstructure examined. Interparticle spacing as low as that obtained would suggest that a material such as this might lend itself to fabrication as a dispersion-strengthened product. The silicon alloy, however, had a somewhat larger average interparticle spacing of 6 microns, an average particle size of 0.4 micron, and a volume percent of oxide of 7.5. Such spacings and sizes are not as fine as would be desired for dispersion-strengthened products. The SAP analog alloy material should have an interparticle spacing of the order of 0.3 micron and particle sizes of the order of 0.02 micron. It is believed, however, that materials with more idealized structures could be produced by variations in thermal and/or mechanical treatment. In fact, other investigators (ref. 7) have produced silicon-bearing copper-base product with particles as fine as 0.04 micron by internal oxidation. They have also produced finely dispersed (0.01 μ) aluminum oxide in copper by an internal oxidation process.

TABLE II. - FREE ENERGIES OF FORMATION OF STABLE METALLIC OXIDES PER MOLE OXYGEN AT 1800° F

Oxide	Free energy of formation, ΔG	Oxide	Free energy of formation, ΔG
NiO	-59.1	Ti_3O_5	-182.0
Al_2O_3	-202.9	TiO_2	-171.4
MgO	-226.7	Cr_2O_3	-129.0
SiO_2	-156.2	MnO	-140.1
TiO	-190.9	Mn_3O_4	-112.9
Ti_2O_3	-187.3	Mn_2O_3	-101.4
		MnO_2	$\lvert\Delta G\rvert < 81$

Thermodynamic considerations. - Small interparticle spacings and particle sizes are desirable in dispersephase strengthened materials. The dispersoids must also satisfactorily resist agglomeration, a process which tends to increase both interparticle spacing and particle size. The tendency of oxide dispersoids to agglomerate is opposed by their inherent stability. This, in turn, may be measured qualitatively by the relative values of free energy of oxide formation. Such values, based on 1 mole of oxygen, were calculated for the solutes employed herein by using the data of reference 18. Table II indicates that magnesium oxide has the largest

(negative) free energy of formation whereas silicon dioxide does not demonstrate an outstandingly large value in this respect. Subscale oxides of the nickel - 0.98-atomic-percent silicon alloy exhibited a relatively fine particle size which was not appreciably affected by the stability heat treatment. However, another alloy with solute oxides having larger free energies of formation displayed evidences of agglomeration. It is evident and important to note, therefore, that the free energy of oxide formation cannot be the sole criterion which governs particle stability in internally oxidized dispersion-strengthened products.

Inherent microstructural considerations associated with the internal oxidation mechanism. - It might be expected that the oxide stability of the dispersion-strengthened product should be enhanced if the oxide dispersoids were all spheroids of approximately the same size. Furthermore, it may be assumed that the gross strength of dispersion-strengthened products would be greater if there were less banding and greater uniformity of dispersion of particles. Hence, the processes by which such heterogeneous configurations may be prevented from forming should be explored. Three of the main potentially troublesome types of dispersoids producible by internal oxidation are illustrated schematically in figure 12. Figure 12(a) shows an external scale and a subscale consisting of dispersoids having a relatively uniform front, but with larger dispersoids at the grain boundaries. On extruding or rolling such a product, the microstructure would be expected to exhibit banding with large particles within the bands. Figure 12(b) illustrates another observation that has been made in this investigation; namely, particle sizes of bulk-diffused materials (i.e., those wherein the oxides were formed on a relatively uniform front) may also vary from large to small. It was noted previously that the large particles might occur away from the outer edge of the specimen and at the farthest point of penetration into the specimen; in other cases, they might form at or near the outer edge adjacent to the surface scale. Differences in oxide particle sizes from the external surface of the material to the inside could in this case also contribute to a heterogeneous structure after working. Still a third type of penetration that may be undesirable is shown in figure 12(c). Here there is an obvious increase in oxide penetration at the grain boundaries. These "prongs," or advance penetrations produced in the grain boundaries relative to the penetrations produced in the bulk of the specimen, can also cause heterogeneity of the structures. Some of these configurations can be prevented by variations of the heat-treating temperatures. For example, in the Ni-Al alloys that were internally oxidized, grain boundary penetration of aluminum oxide was eliminated by raising the temperature from 1500° to 1800° F.

Possibilities for Future Development

Dispersion-strengthened products have been made by internal oxidation processes and in some cases have exhibited very good properties relative to alloys made from comparable base materials. Areas for future work might include the formation of internal carbides or nitrides by diffusion of carbon or nitrogen into a matrix and the subsequent reaction of these materials with alloying additives. Although the free energies of these compounds are generally lower than those of the corresponding oxides, there is a possibility that the morphological characteristics of such products produced in situ in the matrix could outweigh the factors of stability as measured by free energy consider-

ations. In the case of carbides, for example, the possible dispersoids that might form could very readily strengthen superalloy types of materials. Much more should also be done to understand the factors controlling the morphology of oxides formed by internal oxidation methods. Conditions that will produce optimized microstructures, that is, uniform ultrafine dispersoids, must be determined for different metallic systems in order to produce optimized properties in such systems. Another area of interest would relate to alloys containing more than one reacting metal in solid solution. The double oxides that might be possible in these instances could have different effects on the strength of the products than single oxides. Not only will such information help in the understanding of methods to produce dispersion-strengthened products from complex systems, but it might also contribute to the understanding of the surface oxidation of various complex alloys.

Processes may also be devised that combine internal oxidation and powder metallurgy techniques to provide a dispersion-strengthened product. One of the processes that appears to have great potential is that which involves the internal oxidation of prealloyed powders. This procedure is described in reference 6. The major steps in the fabrication of a product by this technique include the internal oxidation of a prealloyed powder, the removal of external oxide scales, and the subsequent sintering and extrusion operations. Prealloyed powders are now commercially available, and only relatively short times should be required in order to oxidize satisfactorily internally fairly large alloy powders. Also, the undesirable external oxide scale normally formed during the internal oxidation process could be kept to a minimum by oxidizing the powders in a low partial pressure of oxygen without adversely affecting the subscale formed. It has been shown that the characteristics of subscale formation in solid-solution Ni-Al alloys are nearly independent of oxygen pressure and that the amount of external scale decreases with decreasing oxygen pressure over the range of 10 to 10^{-4} atmosphere (ref. 19). Finally, extrusion of the sintered internally oxidized material can extend the number of useful alloy systems. For example, the intermediate solute concentration Ni-Al alloys (figs. 5(b) and (c)) might be satisfactory if the platelet structure could be effectively broken up by the extrusion process.

SUMMARY OF RESULTS

The following results were obtained from an investigation of the internal oxidation of a series of nickel-base solid-solution binary alloys. The solute metals were aluminum, magnesium, silicon, titanium, chromium, and manganese. All alloys were oxidized for 200 hours at either 1200°, 1500°, or 1800° F. The subscale oxides so formed were subsequently subjected to a stability heat treatment of 24 hours at 2000° F in vacuum.

1. The depth of subscale penetration increased, both with decreasing solute concentration and increasing oxidation temperatures. Penetrations ranged from a negligible amount to approximately 850 microns after the oxidation treatment.

2. Surface scales found in oxidizing treatments tended to decompose during stability annealing treatments in the vacuum atmosphere to further oxidize the

specimens. In low-temperature oxidation treatments, where no internal oxides were initially observed, the stability treatments produced large internally oxidized zones.

3. Stability anneals at higher than the initial oxidizing temperature in some cases caused relatively little change in shape and size of the original (as-oxidized) internal oxides produced.

4. The morphology of the subscales developed included small, closely spaced particles (i.e., Ni-Mg alloys), highly acicular, oriented particles (i.e., Ni-Al alloys), and large, widely spaced angular shaped oxides (i.e., Ni-Cr and Ni-Mn alloys).

5. Based on optical microscopy, two alloys, the nickel - 1.32-atomic-percent magnesium and the nickel - 0.98-atomic-percent silicon alloys appeared to be particularly amenable to application as dispersion-strengthened materials. The subscales developed in these alloys exhibited microstructures in the as-oxidized conditions with characteristics analogous to those found in aluminum-SAP products. Particle sizes of 0.11 and 0.4 micron and interparticle spacings of 0.73 and 6 microns, respectively, were measured from electron micrographs of these alloys.

CONCLUDING REMARKS

Some interesting observations may be drawn from the results of this study that may facilitate the design and development of dispersion-strengthened alloys. Internal oxidation treatments such as those utilized in this investigation may be applied to bulk materials or to powdered alloys. The data presented may be utilized to approximate the depth of oxide penetration in alloys of similar compositions to those of this study but exposed to different times and temperatures. Also, heat treatments subsequent to the initial oxidation treatment together with variations in solute content may be employed to produce desired morphology. Finally, fine structures such as the acicular precipitates of oxides could probably be fragmented and dispersed in a dispersion-strengthened product by such mechanical processing methods as extrusion or rolling.

Lewis Research Center,
National Aeronautics and Space Administration,
Cleveland, Ohio, February 15, 1965.

REFERENCES

1. Rhines, F. N.: Internal Oxidation. Corrosion and Material Protection, vol. 4, Mar.-Apr., 1947, pp. 15-20.

2. Rhines, F. N.; Johnson, W. A.; and Anderson, W. A.: Rates of High-Temperature Oxidation of Dilute Copper Alloys. AIME Trans., vol. 147, 1942, pp. 205-221.

3. Darken, L. S.: Diffusion in Metals Accompanied by Phase Change. AIME Trans., vol. 150, 1942, pp. 157-171.

4. Meijering, J. L.; and Druyvesteyn, M. J.: Hardening of Metals by Internal Oxidation, pts. I and II. Phillips Research Reports, vols. 1-2, no. 2, 1947, pp. 81-102; pp. 260-280.

5. Irmann, R.: Sintered Aluminum with High Strength at Elevated Temperatures. Metallurgia, vol. 46, Sept. 1952, pp. 125-133.

6. Preston, O.; and Grant, N. J.: Dispersion Strengthening of Copper by Internal Oxidation. AIME Trans., Feb. 1961, vol. 221, pp. 164-173.

7. Komatsu, N.; Bonis, L. J.; and Grant, N. J.: Some Features of Internal Oxidation of Dilute Copper and Nickel Alloys for Dispersion Strengthening. Powder Met., W. Leszynski, ed., Interscience Pub., 1961, pp. 343-358.

8. Wood, D. L.: Internal Oxidation of Copper-Aluminum Alloys. AIME Trans., vol. 215, 1959, pp. 925-932.

9. Gatti, A.: Some Structure and Properties Studies of Internally Oxidized Copper and Nickel Alloys Processed by Powder Metallurgy Techniques. Rept. No. 56-RL-19-RL-1597, General Electric Co., Aug. 1956.

10. Gatti, A.; and Fullman, R. L.: A Study of the Recrystallization Kinetics and Tensile Properties of an Internally Oxidized Solid-Solution Aluminum-Silver Alloy. AIME Trans., vol. 215, Oct. 1959, pp. 762-769.

11. Martin, J. W.; and Smith, G. C.: A Preliminary Note on the Creep Properties of Internally Oxidized Copper Alloys. J. Inst. Metals, vol. 83, June 1955, pp. 417-420.

12. Bonis, Laszlo J.; and Grant, Nicholas J.: The Structure and Properties of Dispersion Strengthened Internally Oxidized Nickel Alloys. AIME Trans., vol. 224, Apr. 1962, pp. 308-316.

13. Seebohm, R. H.; and Martin, J. W.: The Effect of Internal Oxidation on Some Properties of Copper Alloy Sintered Compacts. Metallurgia, vol. 61, Apr. 1960, pp. 163-166.

14. Rhines, F. N.: A Metallographic Study of Internal Oxidation in the Alpha Solid Solutions of Copper. AIME Trans. vol. 137, 1940, pp. 246-286.

15. Smith, G. C.; and Dewhirst, D. W.: Metallography and Mechanical Properties Internally Oxidized (Copper) Alloys. Research, vol. 2, no. 10, 1949, pp. 492-493.

16. Slade, J. A.; and Martin, J. W.: Ductility in Internally Oxidized Silver Alloys. Metallurgia, vol. 64, July 1961, pp. 23-25.

17. Thomas, D. E.: High Temperature Oxidation of Copper-Palladium and Copper-Platinum Alloys. AIME Trans., vol. 191, 1951, pp. 926-936.

18. Coughlin, J. P.: Contributions to the Data on Theoretical Metallurgy. Pt. XII - Heats and Free Energies of Formation of Inorganic Oxides. Bull. 542, Bur. of Mines, 1954.

19. Wolf, J. S.; and Evans, E. B.: Effect of Oxygen Pressure on Internal Oxidation of Nickel-Aluminum Alloys. Corrosion, vol. 18, no. 4, Apr. 1962, pp. 129t-136t.

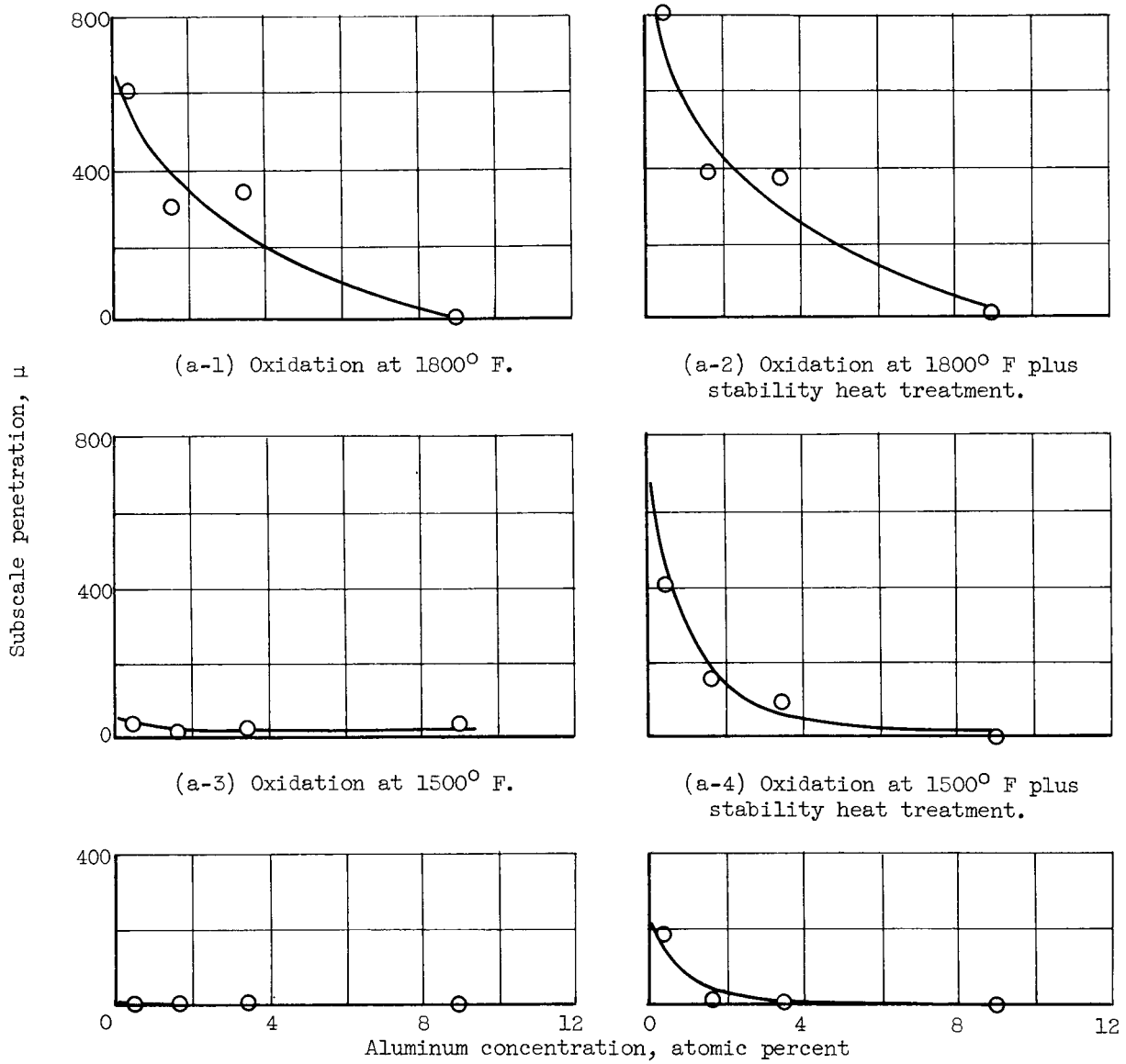

(a) Nickel-aluminum alloys.

Figure 1. - Subscale penetration in various nickel-base binary alloys as function of solute concentration after oxidation for 200 hours at 1800°, 1500°, and 1200° F before and after stability heat treatment.

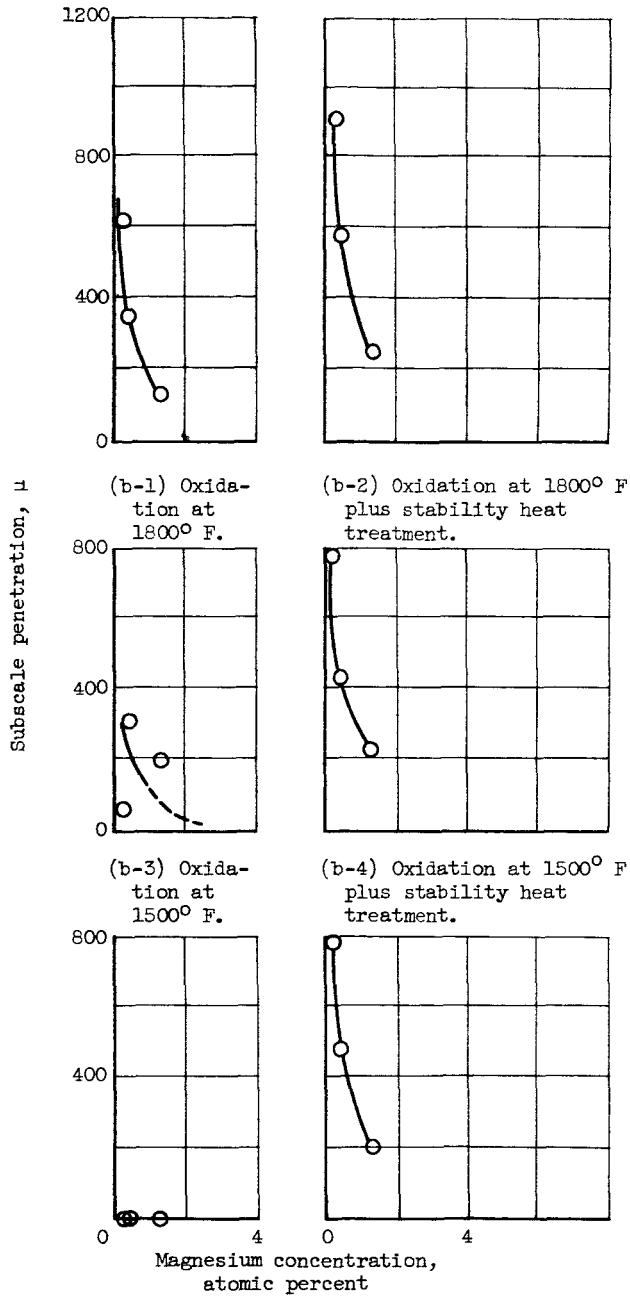

(b) Nickel-magnesium alloys.

Figure 1. - Continued. Subscale penetration in various nickel-base binary alloys as function of solute concentration after oxidation for 200 hours at 1800°, 1500°, and 1200° F before and after stability heat treatment.

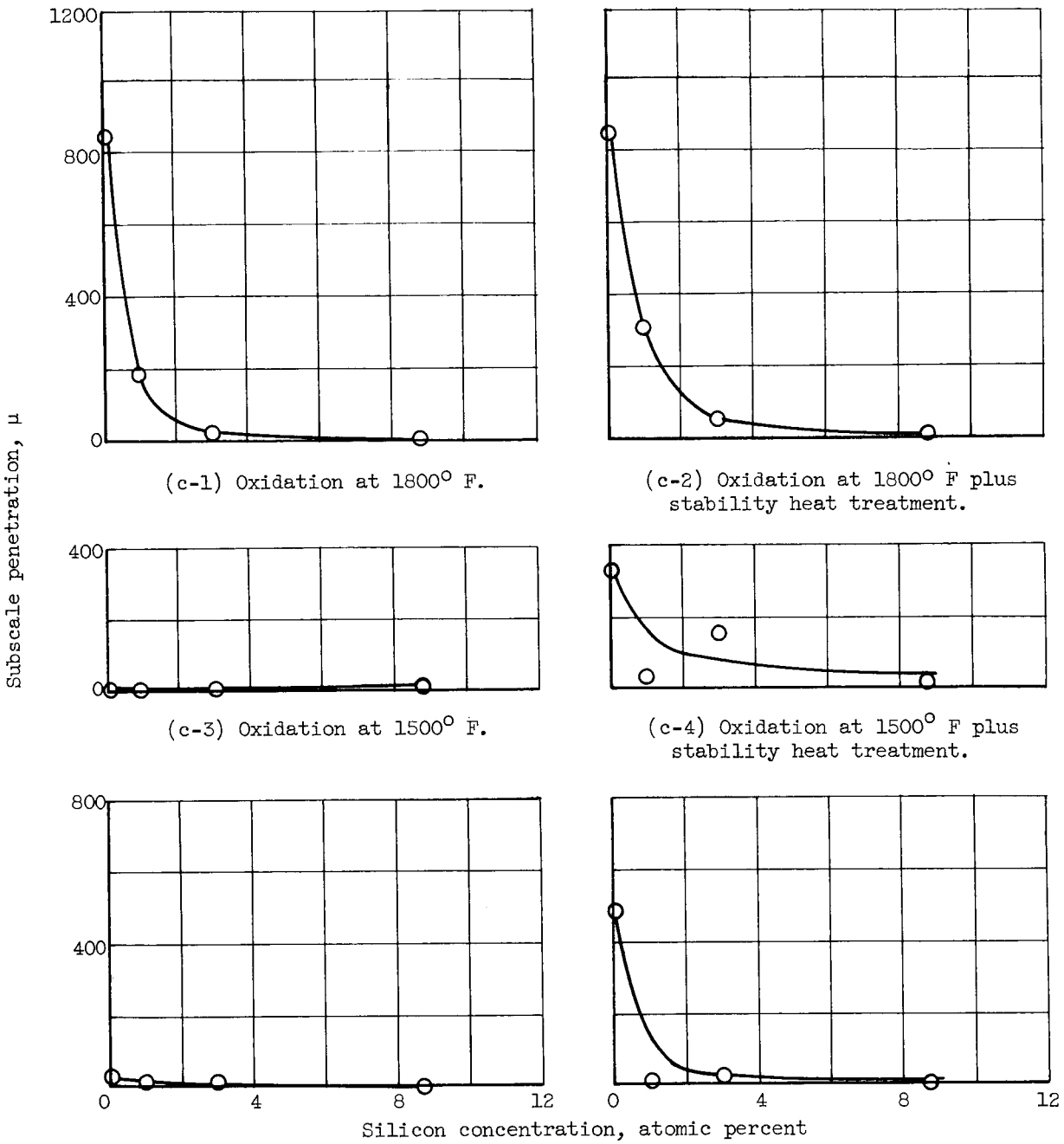

(c-1) Oxidation at 1800° F.

(c-2) Oxidation at 1800° F plus stability heat treatment.

(c-3) Oxidation at 1500° F.

(c-4) Oxidation at 1500° F plus stability heat treatment.

(c-5) Oxidation at 1200° F.

(c-6) Oxidation at 1200° F plus stability heat treatment.

(c) Nickel-silicon alloys.

Figure 1. - Continued. Subscale penetration in various nickel-base binary alloys as function of solute concentration after oxidation for 200 hours at 1800°, 1500°, and 1200° F before and after stability heat treatment.

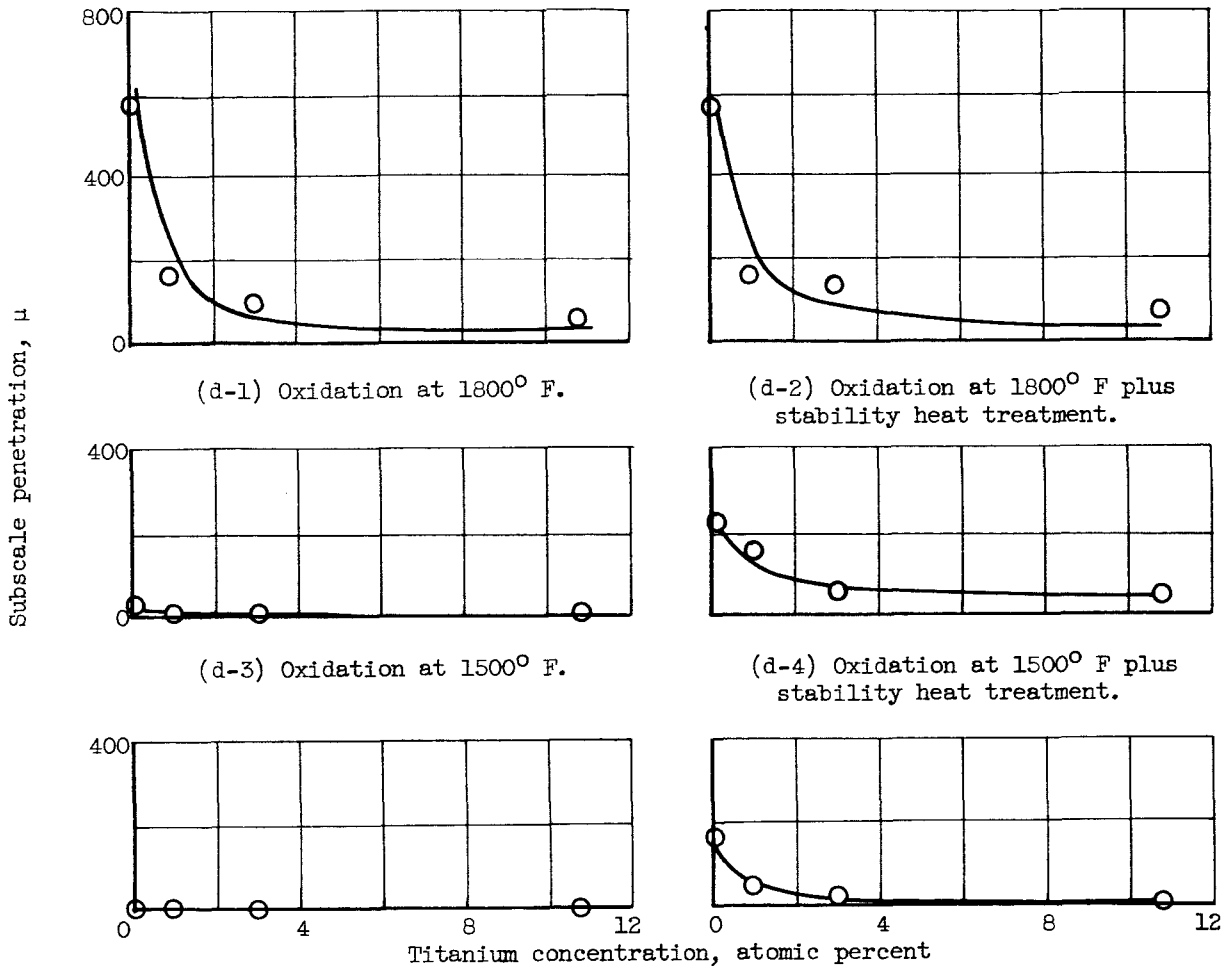

(d-1) Oxidation at 1800° F.

(d-2) Oxidation at 1800° F plus stability heat treatment.

(d-3) Oxidation at 1500° F.

(d-4) Oxidation at 1500° F plus stability heat treatment.

(d-5) Oxidation at 1200° F.

(d-6) Oxidation at 1200° F plus stability heat treatment.

(d) Nickel-titanium alloys.

Figure 1. - Continued. Subscale penetration in various nickel-base binary alloys as function of solute concentration after oxidation for 200 hours at 1800°, 1500°, and 1200° F before and after stability heat treatment.

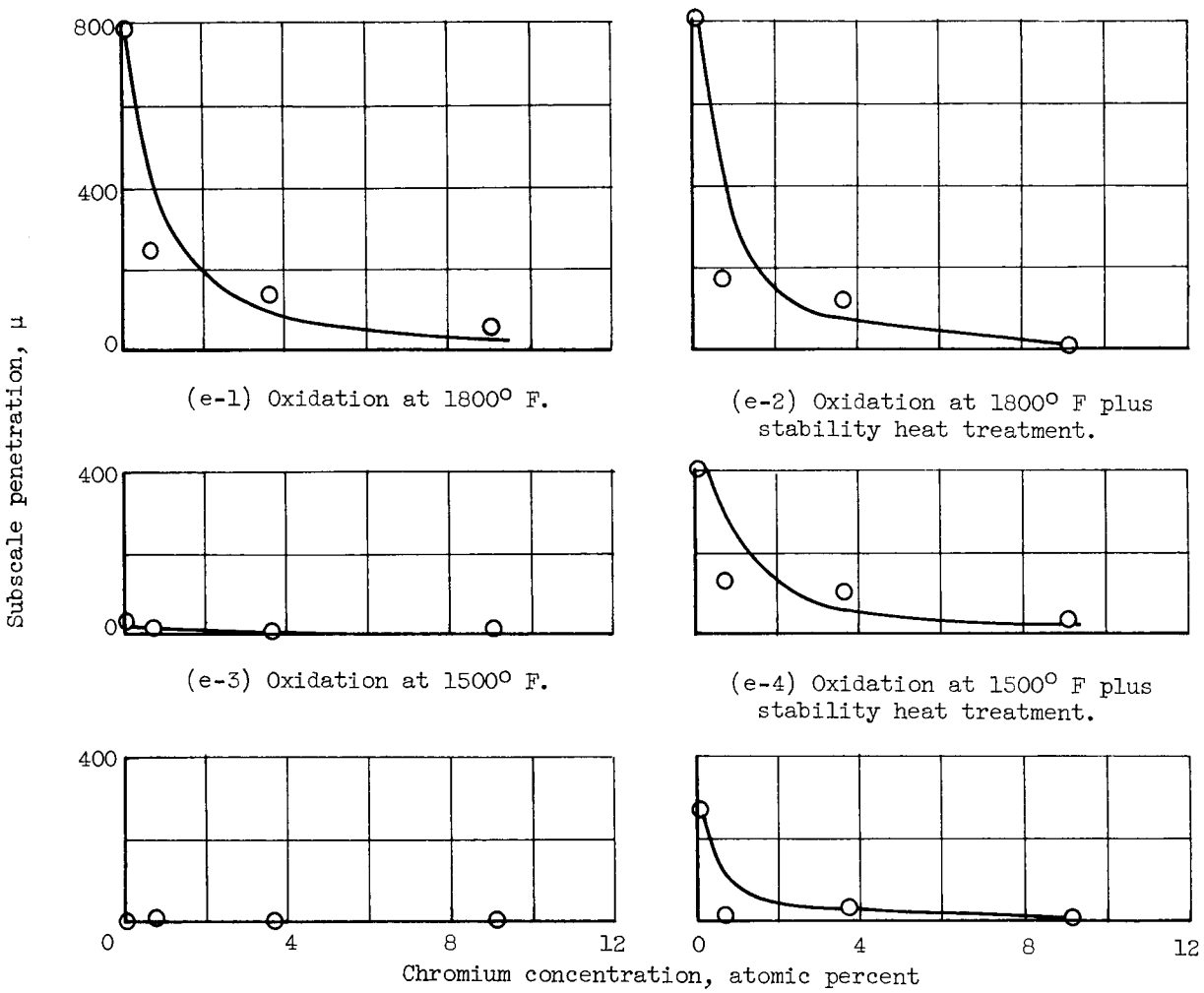

(e-1) Oxidation at 1800° F.

(e-2) Oxidation at 1800° F plus stability heat treatment.

(e-3) Oxidation at 1500° F.

(e-4) Oxidation at 1500° F plus stability heat treatment.

(e-5) Oxidation at 1200° F.

(e-6) Oxidation at 1200° F plus stability heat treatment.

(e) Nickel-chromium alloys.

Figure 1. - Continued. Subscale penetration in various nickel-base binary alloys as function of solute concentration after oxidation for 200 hours at 1800°, 1500°, and 1200° F before and after stability heat treatment.

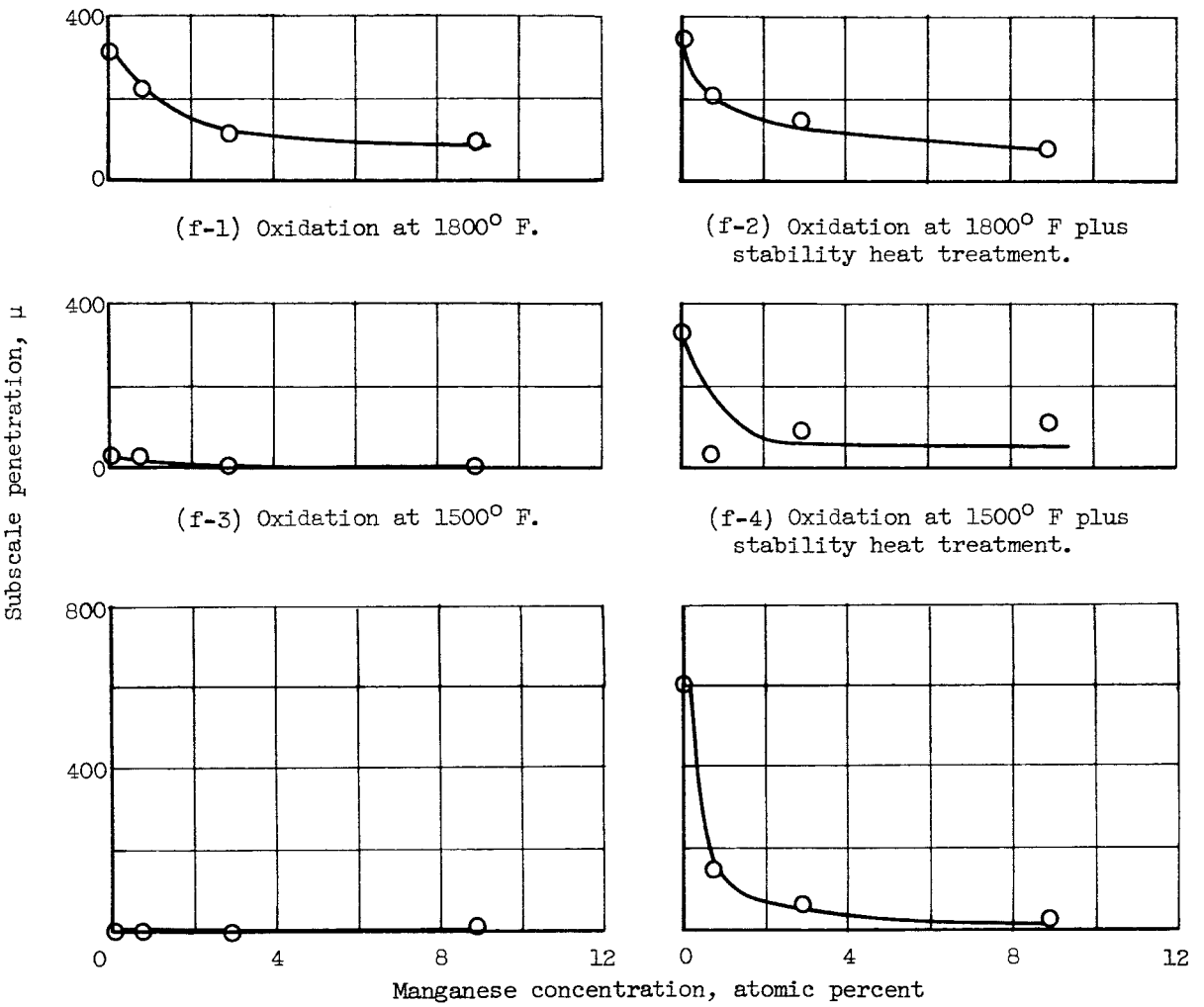

(f-1) Oxidation at 1800° F.

(f-2) Oxidation at 1800° F plus stability heat treatment.

(f-3) Oxidation at 1500° F.

(f-4) Oxidation at 1500° F plus stability heat treatment.

(f-5) Oxidation at 1200° F.

(f-6) Oxidation at 1200° F plus stability heat treatment.

(f) Nickel-manganese alloys.

Figure 1. - Concluded. Subscale penetration in various nickel-base binary alloys as function of solute concentration after oxidation for 200 hours at 1800°, 1500°, and 1200° F before and after stability heat treatment.

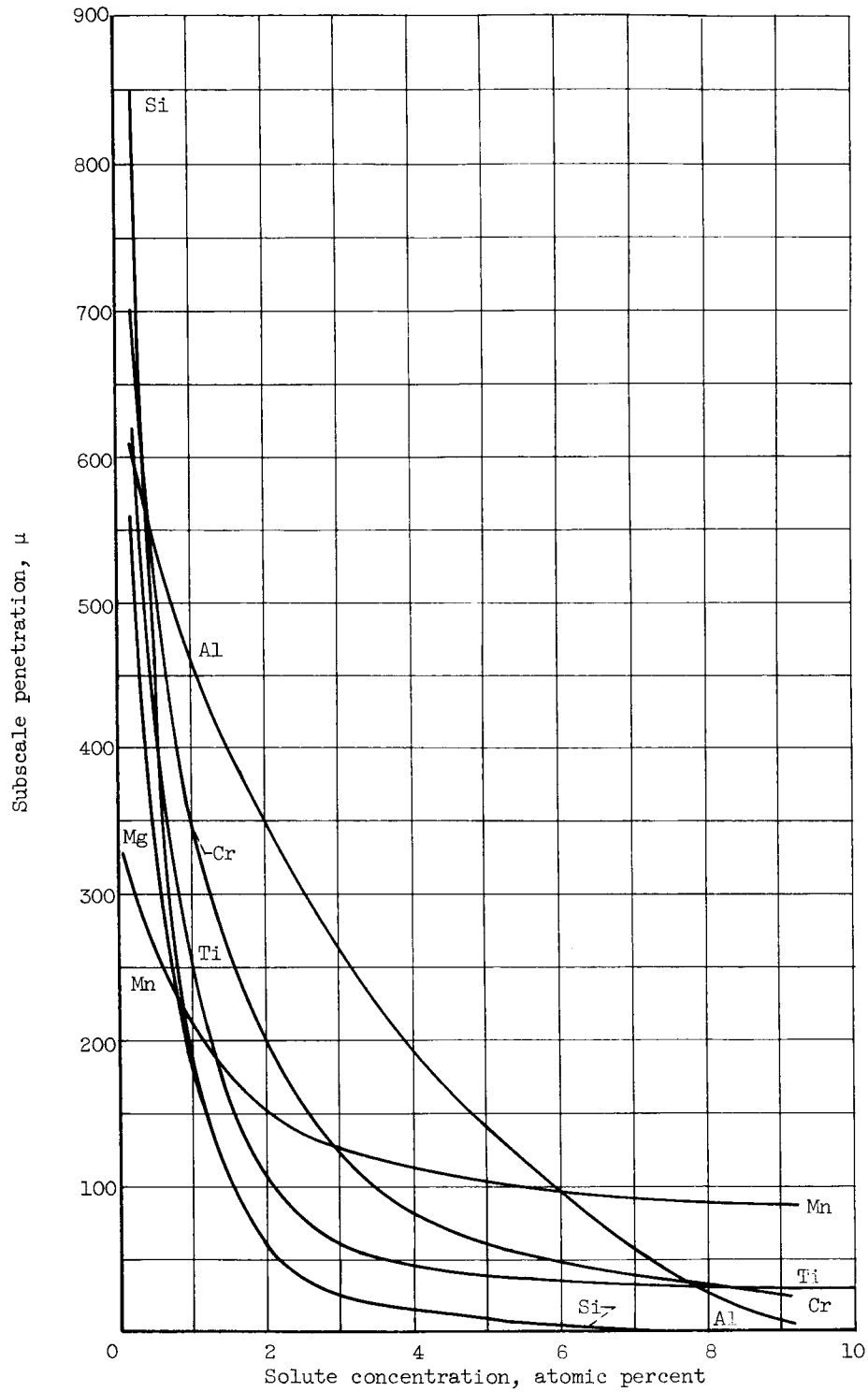

Figure 2. - Summary plot of subscale penetration in various nickel-base binary alloys as function of solute concentration after oxidation for 200 hours at 1800° F.

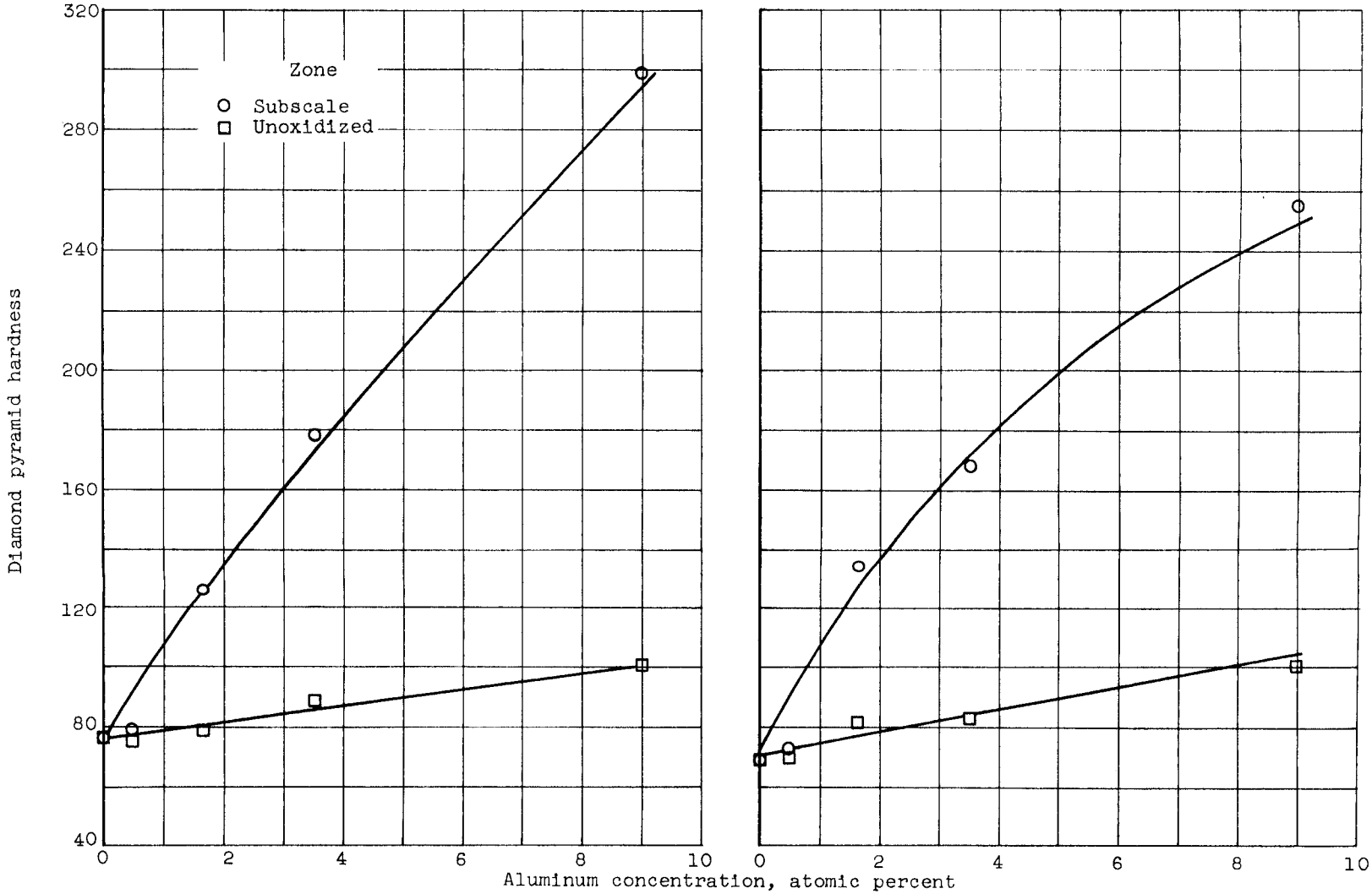

(a-1) Oxidation at 1800° F.

(a-2) Oxidation at 1800° F plus stability heat treatment.

(a) Nickel-aluminum alloys.

Figure 3. - Hardness of subscale and unoxidized zones of various nickel-base binary alloys as function of solute concentration after oxidation for 200 hours at 1800° F before and after stability heat treatment.

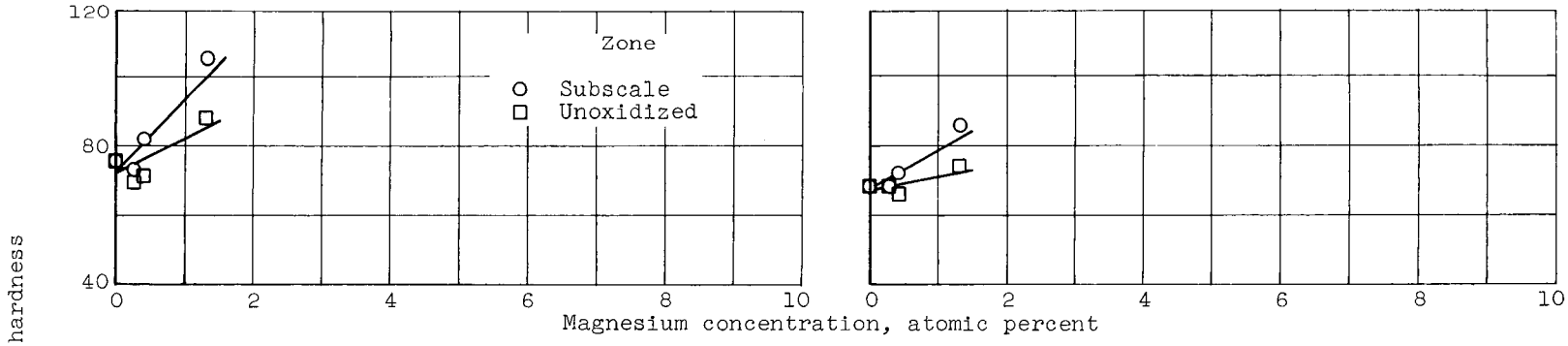

(b-1) Oxidation at 1800° F.

(b-2) Oxidation at 1800° F plus stability heat treatment.

(b) Nickel-magnesium alloys.

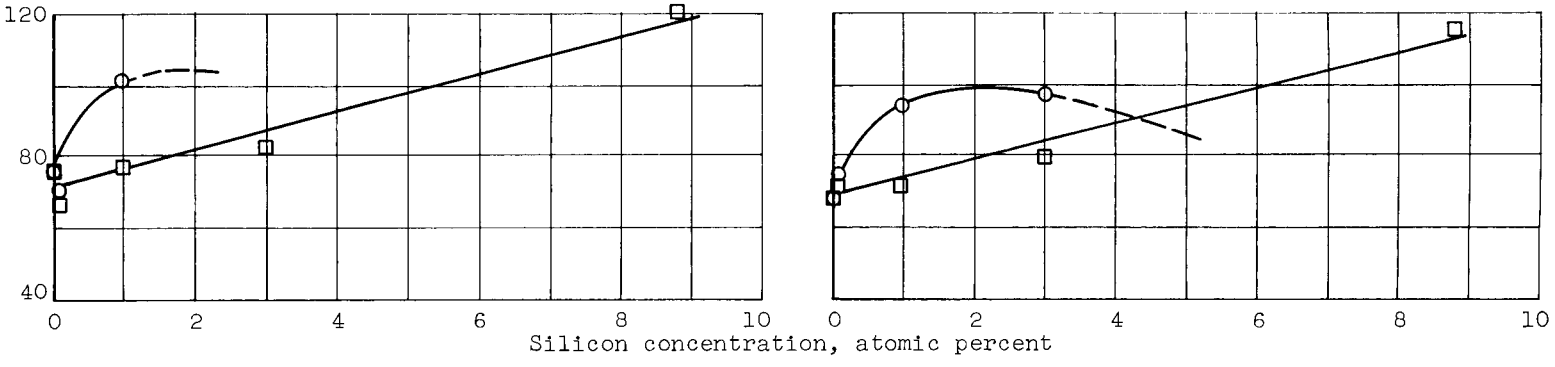

(c-1) Oxidation at 1800° F.

(c-2) Oxidation at 1800° F plus stability heat treatment.

(c) Nickel-silicon alloys.

Figure 3. - Continued. Hardness of subscale and unoxidized zones of various nickel-base binary alloys as function of solute concentration after oxidation for 200 hours at 1800° F before and after stability heat treatment.

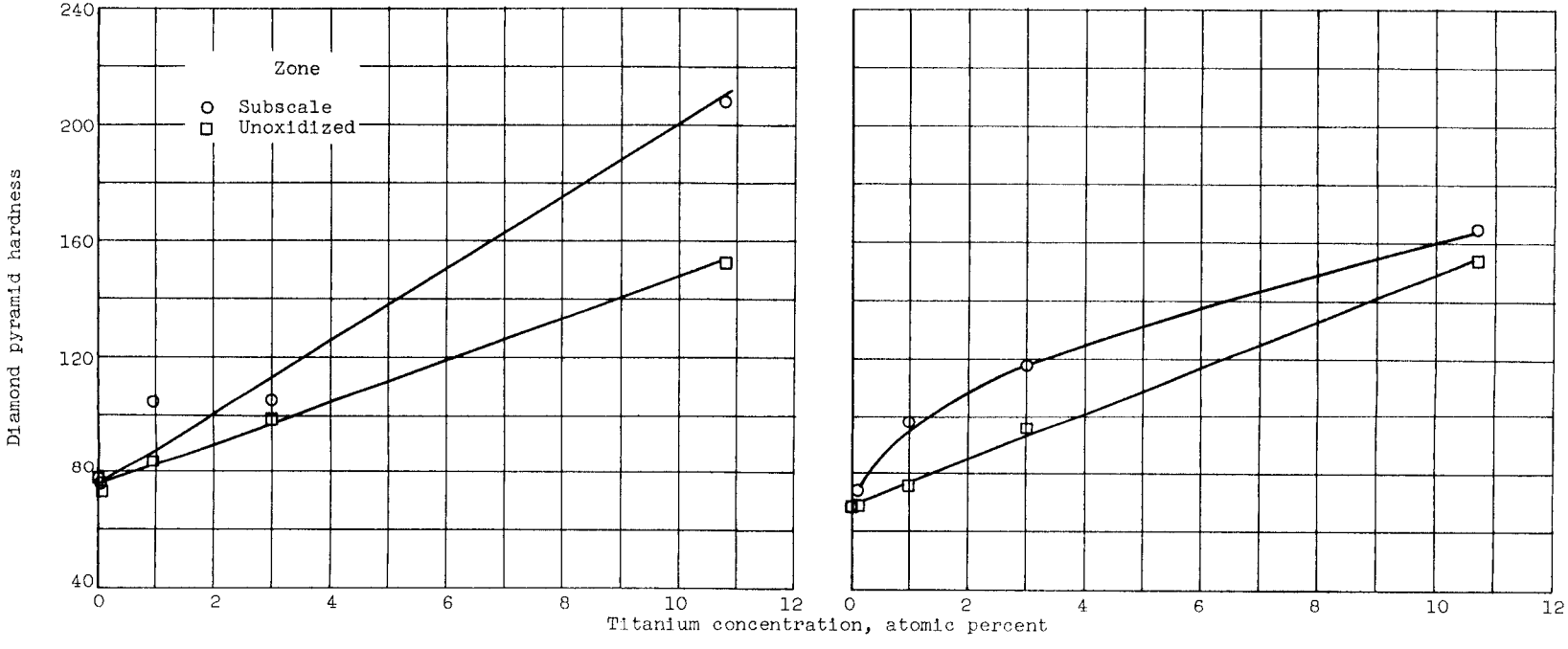

(d-1) Oxidation at 1800° F.

(d-2) Oxidation at 1800° F plus stability heat treatment.

(d) Nickel-titanium alloys.

Figure 3. - Continued. Hardness of subscale and unoxidized zones of various nickel-base binary alloys as function of solute concentration after oxidation for 200 hours at 1800° F before and after stability heat treatment.

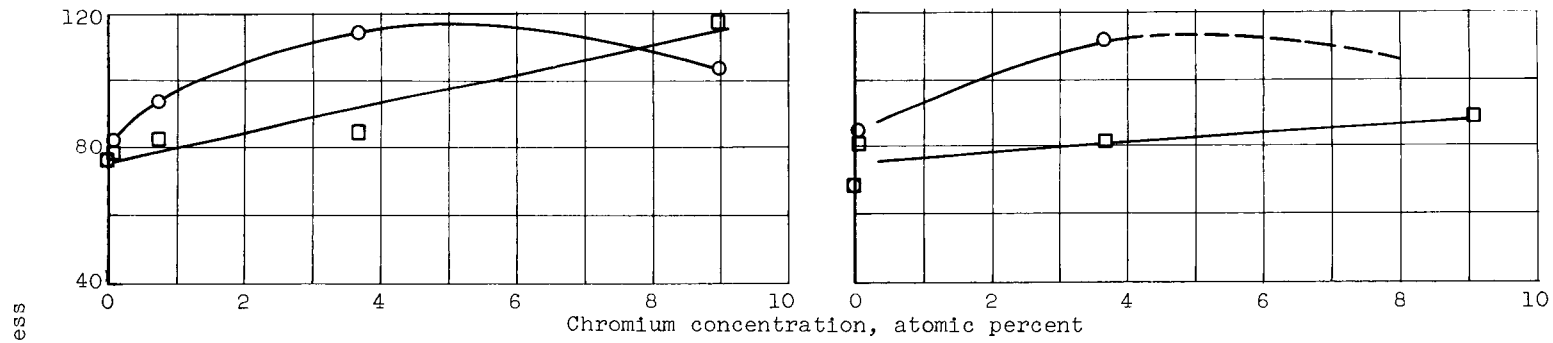

(e-1) Oxidation at 1800° F.

(e-2) Oxidation at 1800° F plus stability heat treatment.

(e) Nickel-chromium alloys.

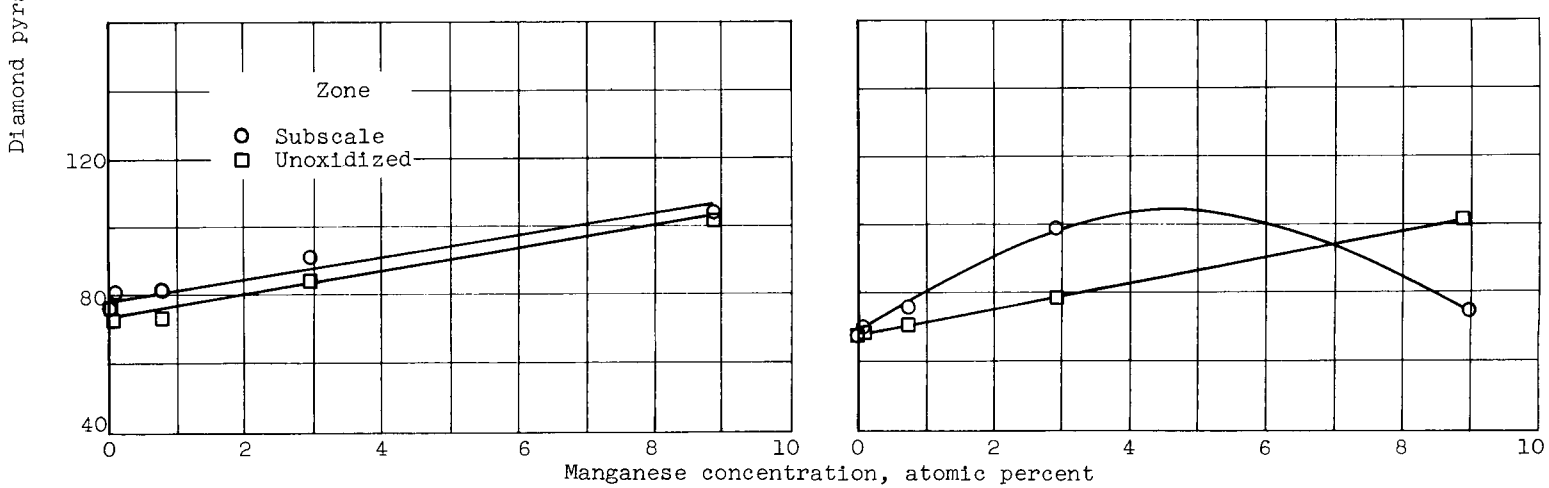

(f-1) Oxidation at 1800° F.

(f-2) Oxidation at 1800° F plus stability heat treatment.

(f) Nickel-manganese alloys.

Figure 3. - Concluded. Hardness of subscale and unoxidized zones of various nickel-base binary alloys as function of solute concentration after oxidation for 200 hours at 1800° F before and after stability heat treatment.

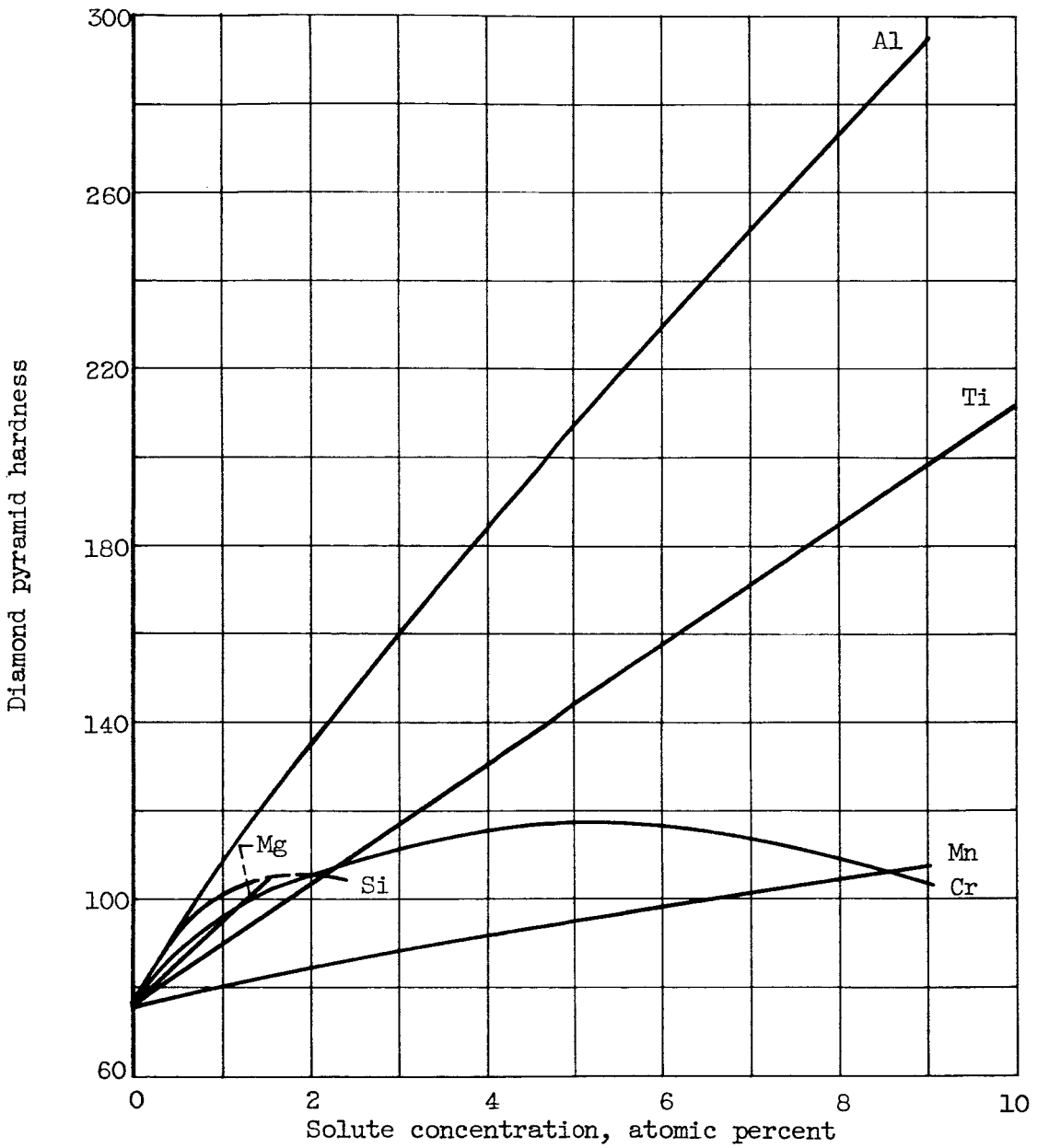

Figure 4. - Summary plot of subscale hardness in various nickel-base binary alloys as function of solute concentration after oxidation for 200 hours at 1800° F.

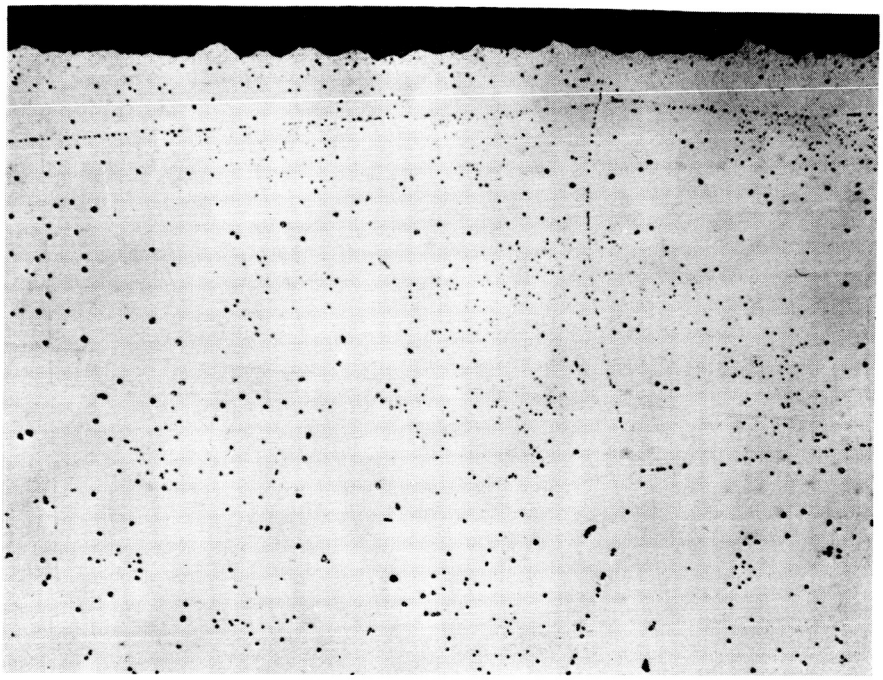

(a-1) As-oxidized.

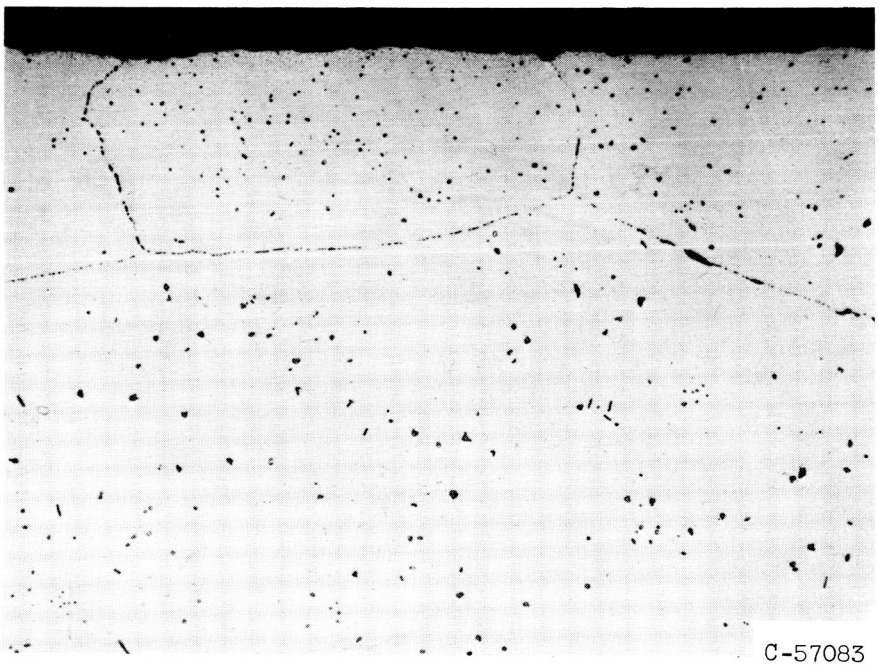

C-57083

(a-2) As-oxidized plus stability heat treatment.

(a) Aluminum content, 0.48 atomic percent; temperature, 1800° F.

Figure 5. - Photomicrographs of nickel-aluminum alloy oxidized for 200 hours before and after stability heat treatment. Marble's etch. ×500.

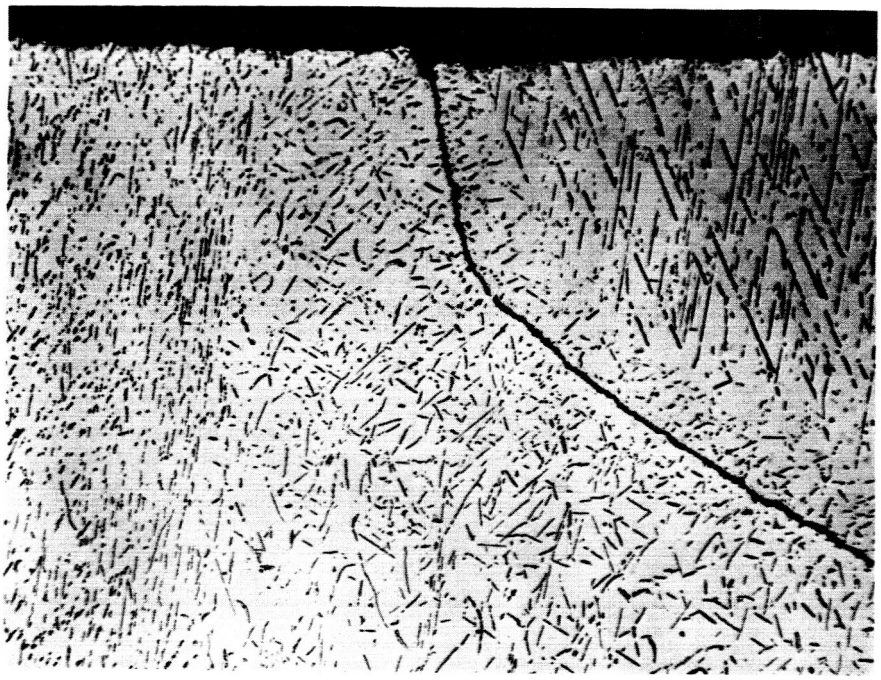

(b-1) As-oxidized.

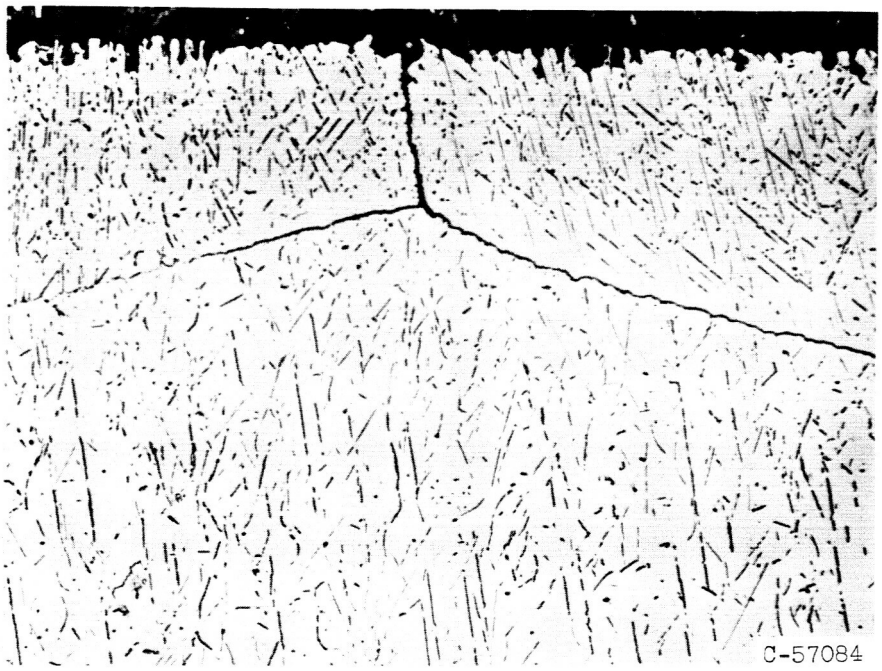

(b-2) As-oxidized plus stability heat treatment.

(b) Aluminum content, 1.66 atomic percent; temperature, 1800° F.

Figure 5. - Continued. Photomicrographs of nickel-aluminum alloy oxidized for 200 hours before and after stability heat treatment. Marble's etch. ×500.

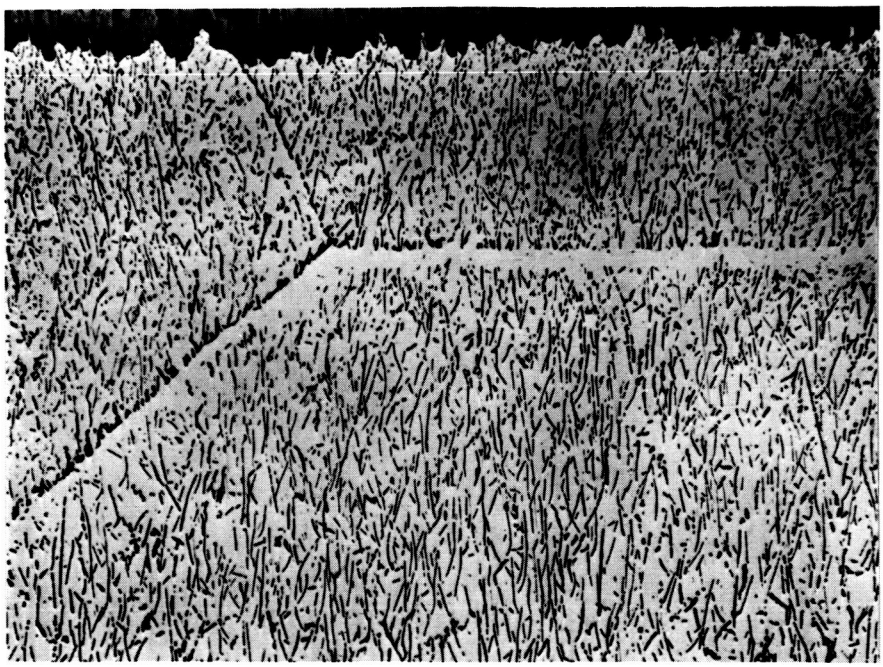

(c-1) As-oxidized.

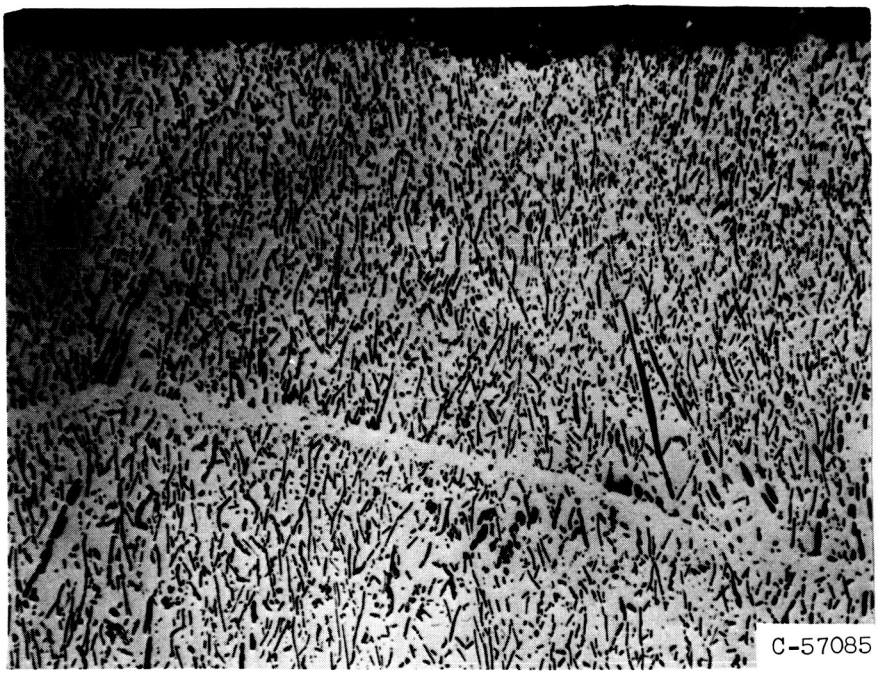

(c-2) As-oxidized plus stability heat treatment.

(c) Aluminum content, 3.52 atomic percent; temperature, 1800° F.

Figure 5. - Continued. Photomicrographs of nickel-aluminum alloy oxidized for 200 hours before and after stability heat treatment. Marble's etch. ×500.

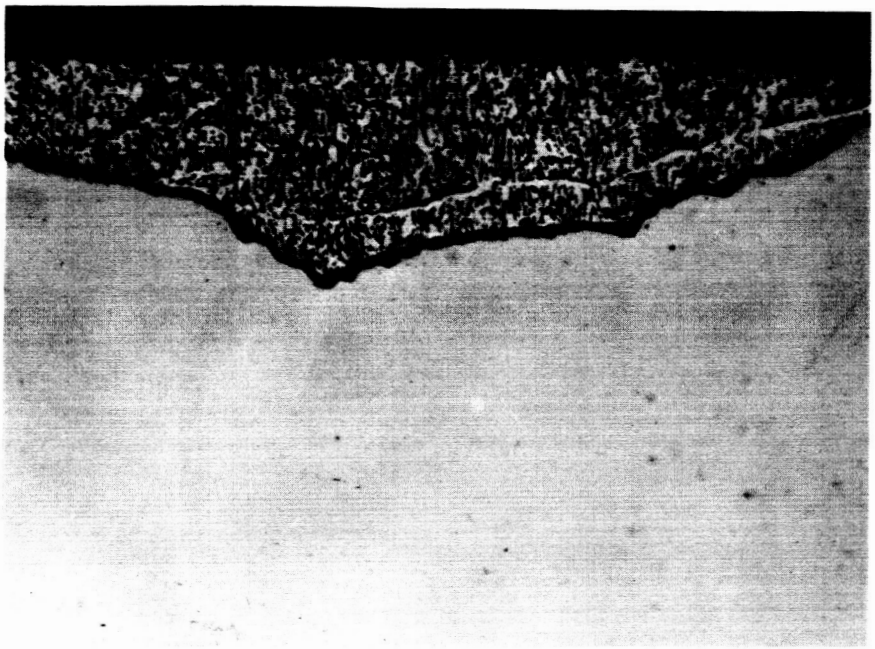

(d-1) As-oxidized.

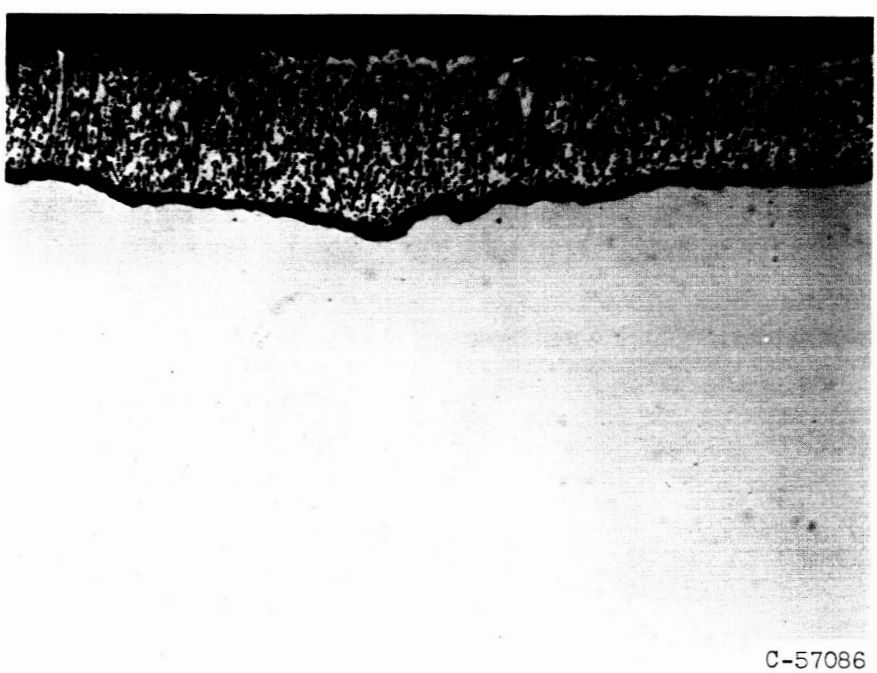

C-57086

(d-2) As-oxidized plus stability heat treatment.

(d) Aluminum content, 9.01 atomic percent; temperature, 1800° F.

Figure 5. - Continued. Photomicrographs of nickel-aluminum alloy oxidized for 200 hours before and after stability heat treatment. Marble's etch. ×500.

(e-1) As-oxidized.

(e-2) As-oxidized plus stability heat treatment.

(e) Aluminum content, 0.48 atomic percent; temperature, 1500° F.

Figure 5. - Continued. Photomicrographs of nickel-aluminum alloy oxidized for 200 hours before and after stability heat treatment. Marble's etch. ×500.

(f-1) As-oxidized.

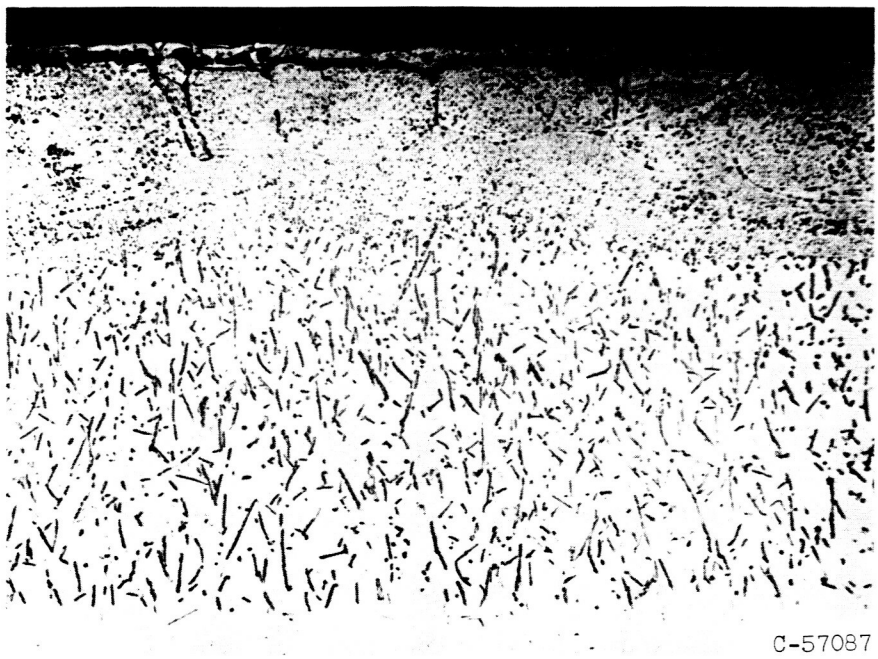

C-57087

(f-2) As-oxidized plus stability heat treatment.

(f) Aluminum content, 1.66 atomic percent; temperature, 1500° F.

Figure 5. - Continued. Photomicrographs of nickel-aluminum alloy oxidized for 200 hours before and after stability heat treatment. Marble's etch. ×500.

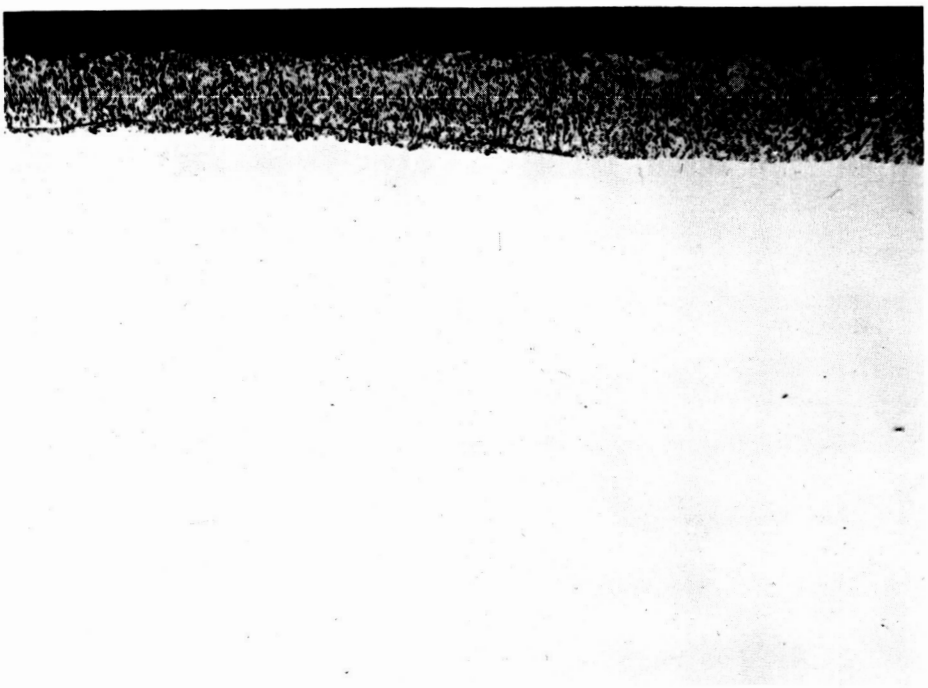

(g-1) As-oxidized.

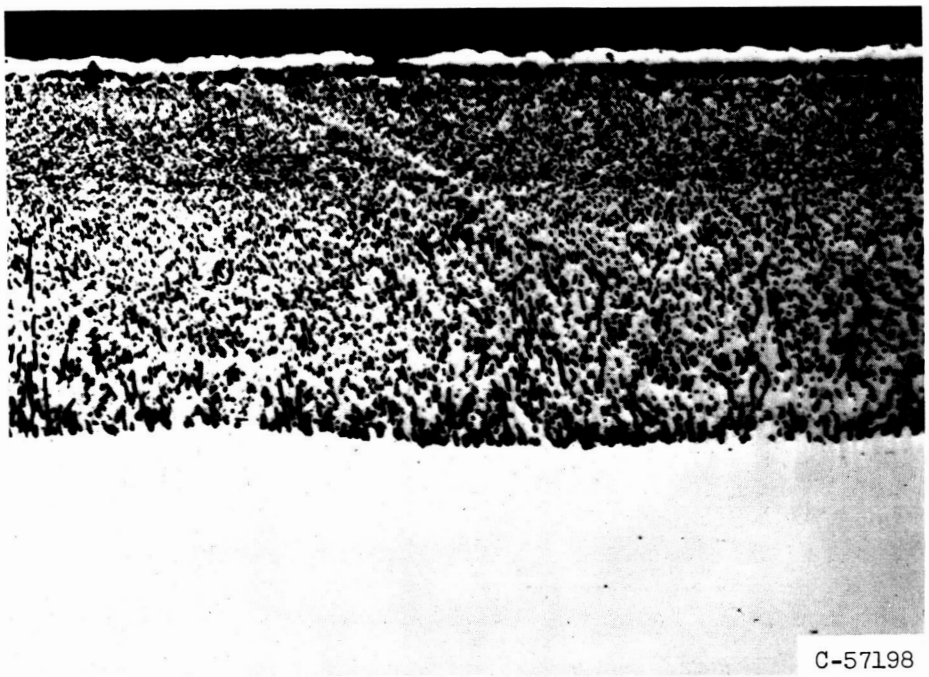

(g-2) As-oxidized plus stability heat treatment.

(g) Aluminum content, 3.52 atomic percent; temperature, 1500° F.

Figure 5. - Continued. Photomicrographs of nickel-aluminum alloy oxidized for 200 hours before and after stability heat treatment. Marble's etch. ×500.

(h-1) As-oxidized.

C-57088

(h-2) As-oxidized plus stability heat treatment.

(h) Aluminum content, 9.01 atomic percent; temperature, 1500° F.

Figure 5. - Continued. Photomicrographs of nickel-aluminum alloy oxidized for 200 hours before and after stability heat treatment. Marble's etch. ×500.

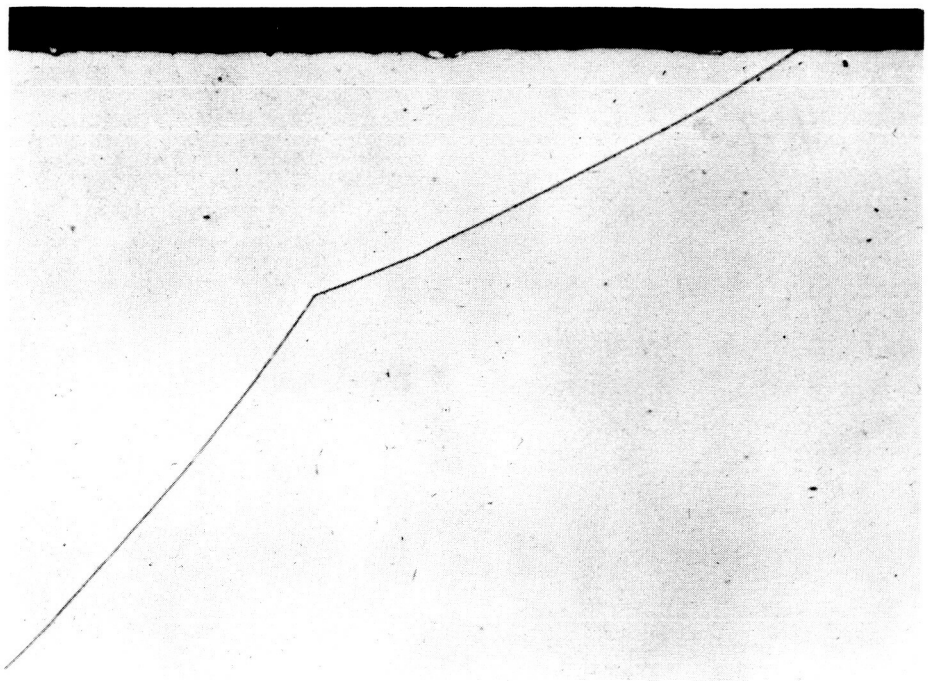

(i-1) As-oxidized.

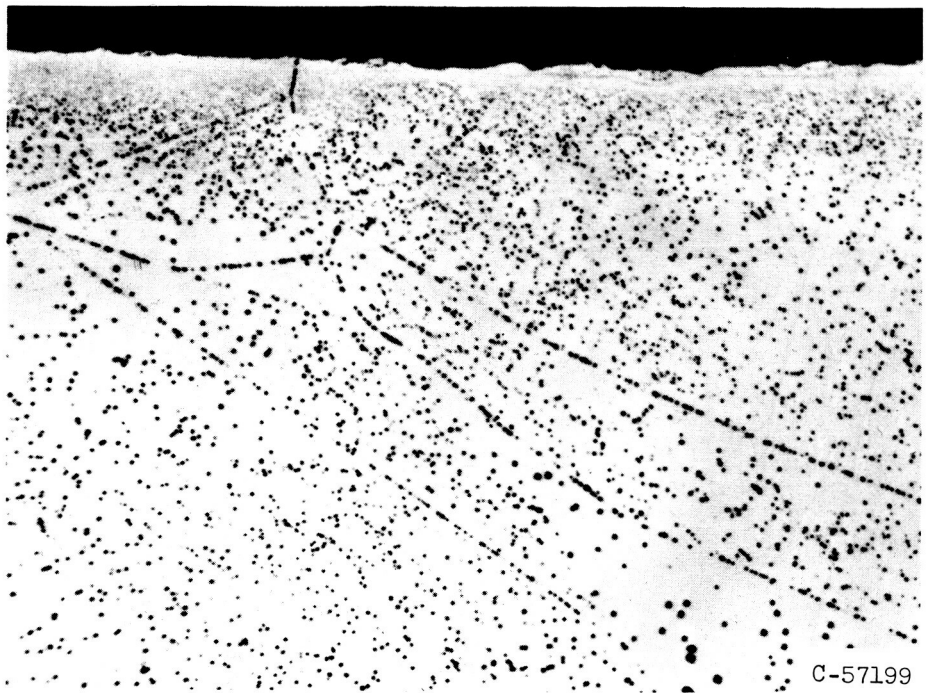

(i-2) As-oxidized plus stability heat treatment.

(i) Aluminum content, 0.48 atomic percent; temperature, 1200° F.

Figure 5. - Continued. Photomicrographs of nickel-aluminum alloy oxidized for 200 hours before and after stability heat treatment. Marble's etch. ×500.

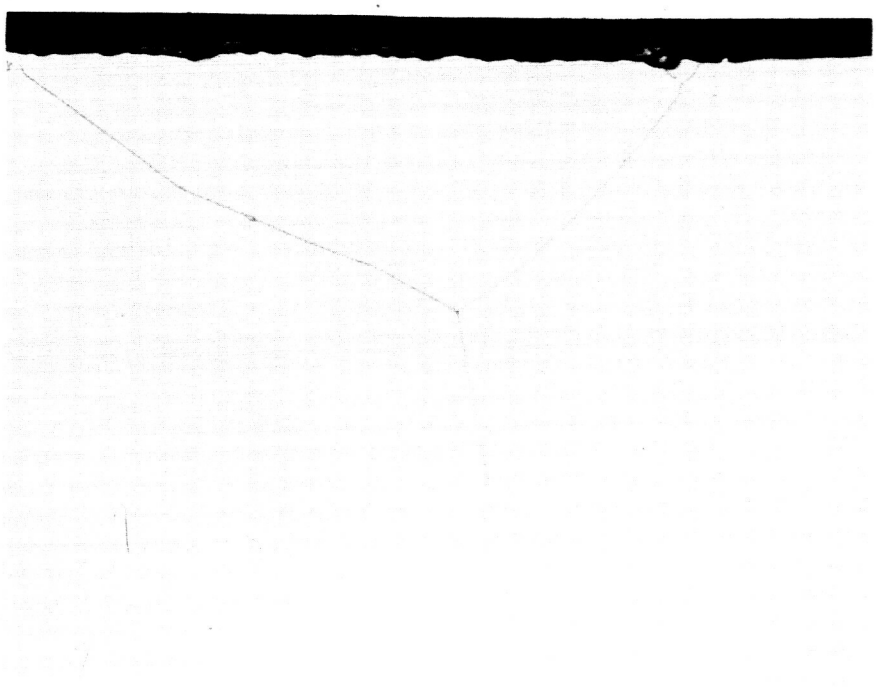

(j-1) As-oxidized.

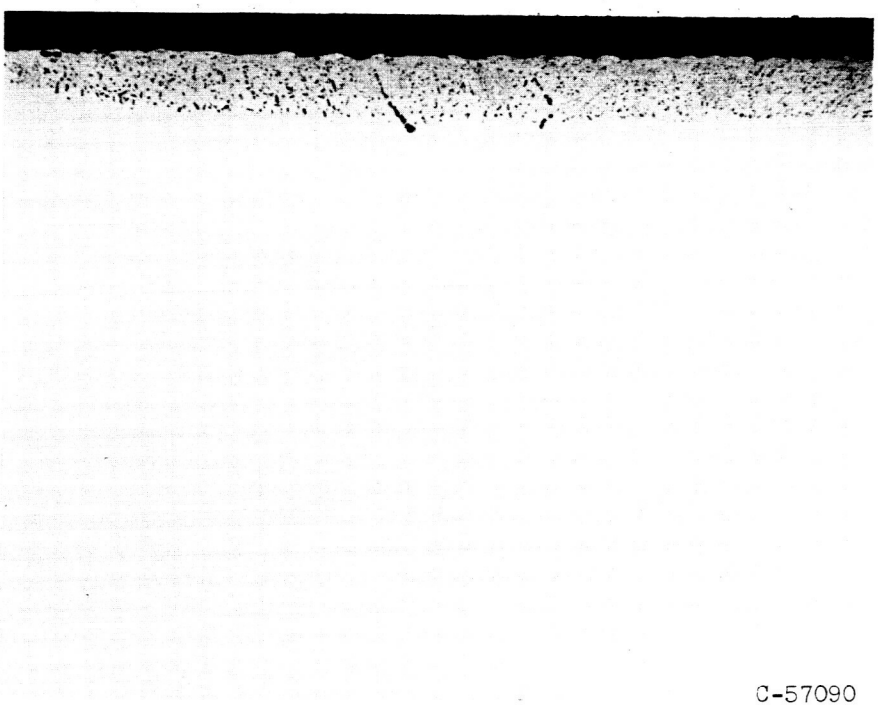

C-57090

(j-2) As-oxidized plus stability heat treatment.

(j) Aluminum content, 1.66 atomic percent; temperature, 1200° F.

Figure 5. - Continued. Photomicrographs of nickel-aluminum alloy oxidized for 200 hours before and after stability heat treatment. Marble's etch. ×500.

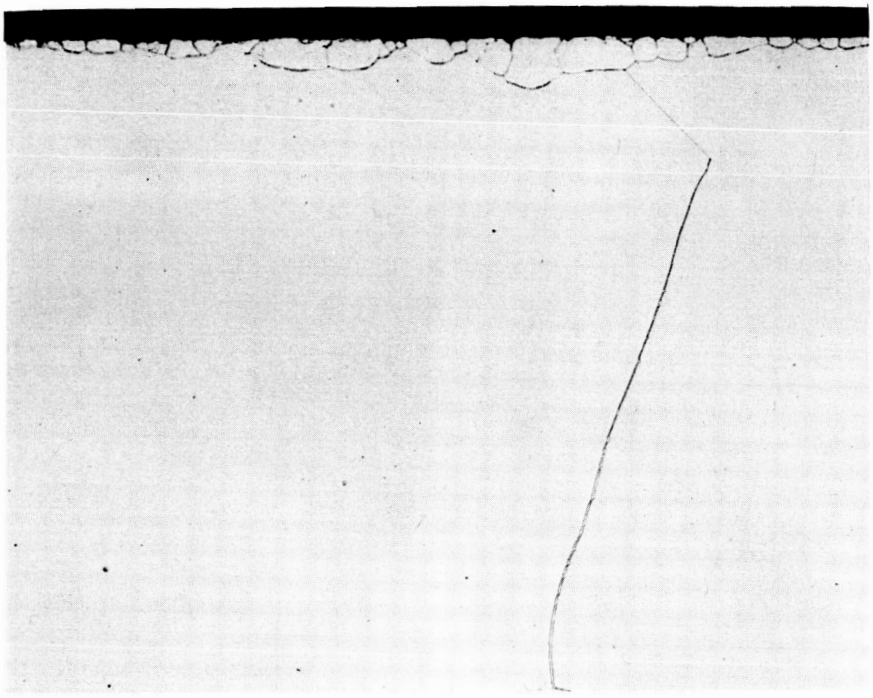

(k-1) As-oxidized.

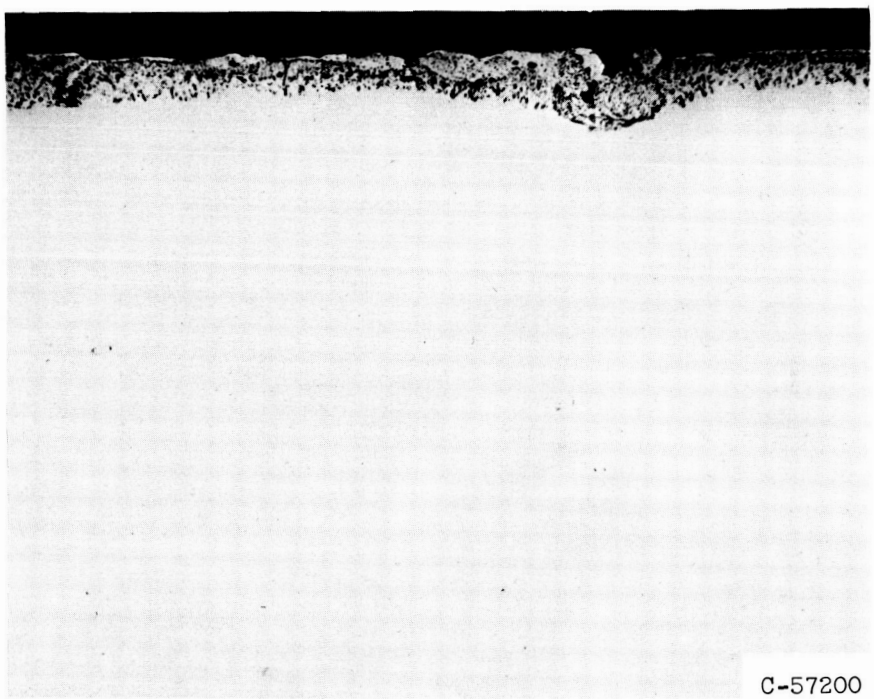

(k-2) As-oxidized plus stability heat treatment.

(k) Aluminum content, 3.52 atomic percent; temperature, 1200° F.

Figure 5. - Continued. Photomicrographs of nickel-aluminum alloy oxidized for 200 hours before and after stability heat treatment. Marble's etch. ×500.

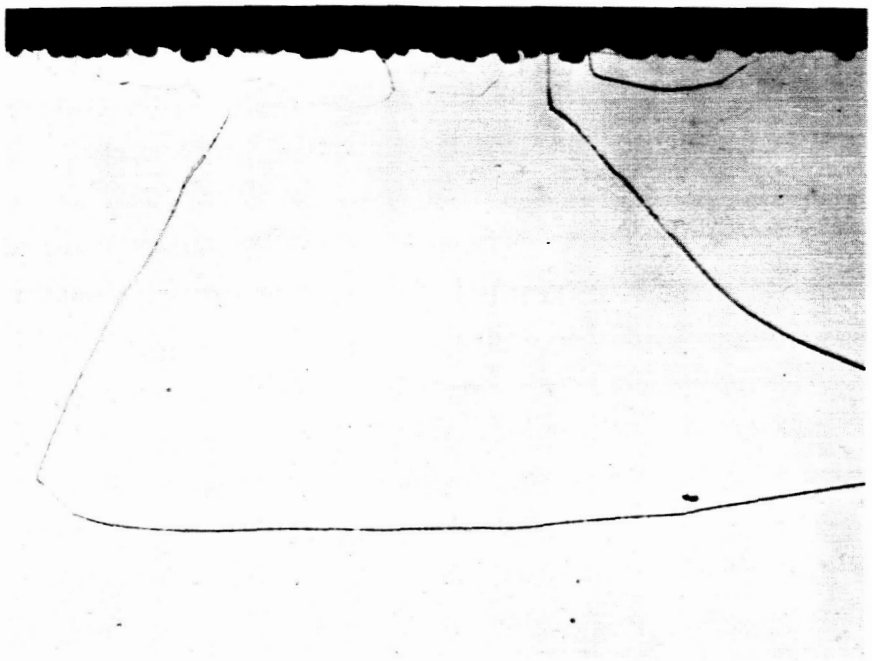

(1-1) As-oxidized.

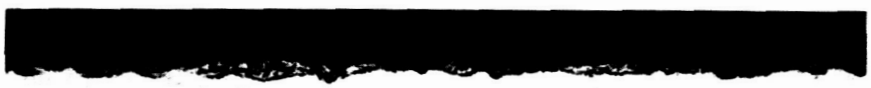

C-57089

(1-2) As-oxidized plus stability heat treatment.

(1) Aluminum content, 9.01 atomic percent; temperature, 1200° F.

Figure 5. - Concluded. Photomicrographs of nickel-aluminum alloy oxidized for 200 hours before and after stability heat treatment. Marble's etch. ×500.

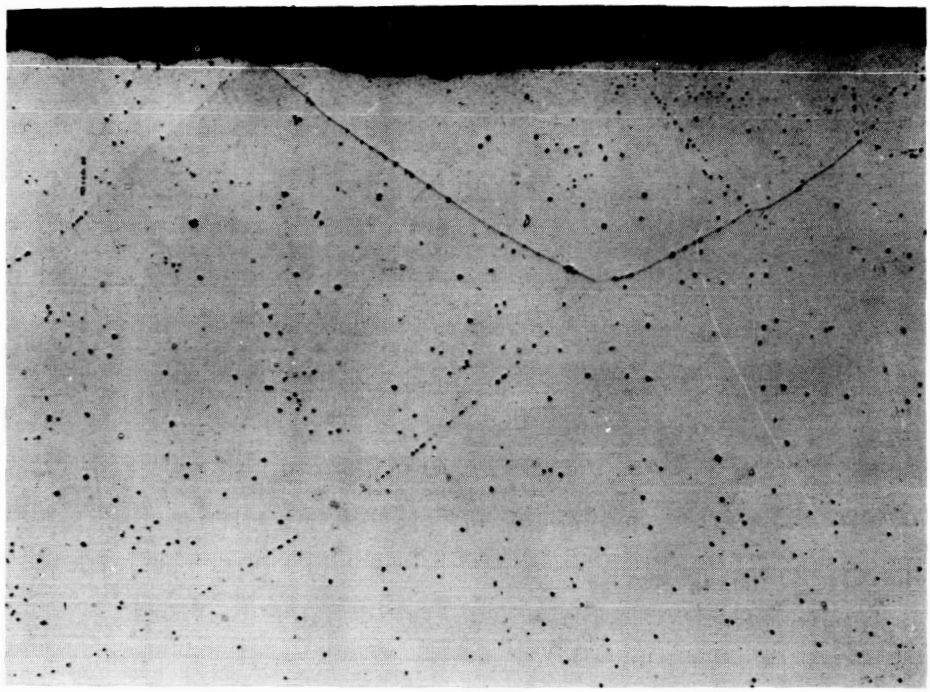

(a-1) As-oxidized.

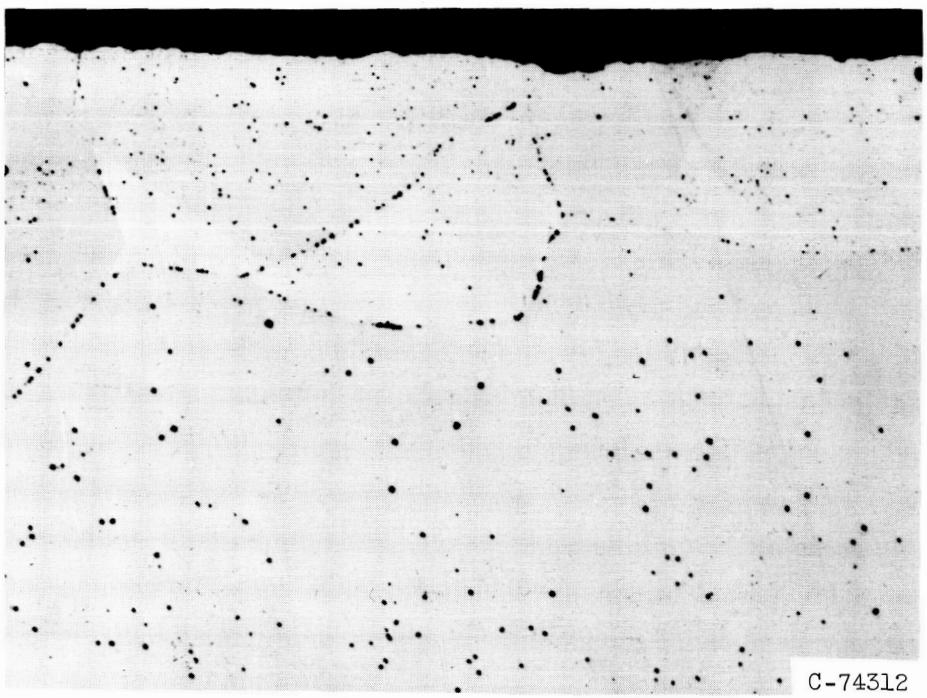

(a-2) As-oxidized plus stability heat treatment.

(a) Photomicrographs; magnesium content, 0.27 atomic percent. ×500.

Figure 6. - Micrographs of nickel-magnesium alloy oxidized for 200 hours at 1800° F before and after stability heat treatment. Marble's etch.

(b-1) As-oxidized.

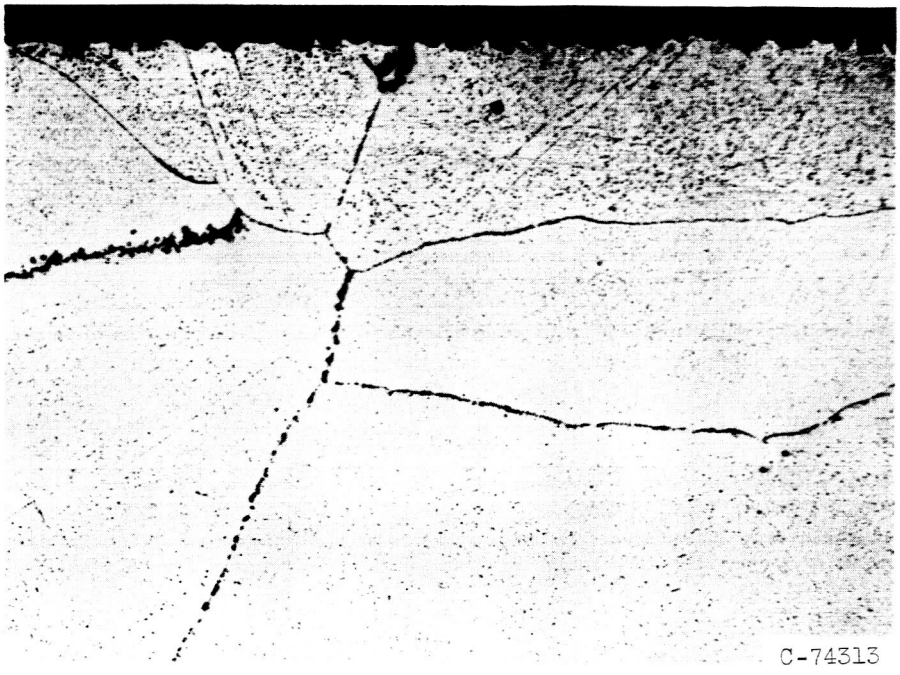

(b-2) As-oxidized plus stability heat treatment.

(b) Photomicrographs; magnesium content, 0.43 atomic percent. ×500.

Figure 6. - Continued. Micrographs of nickel-magnesium alloy oxidized for 200 hours at 1800° F before and after stability heat treatment. Marble's etch.

(c-1) As-oxidized.

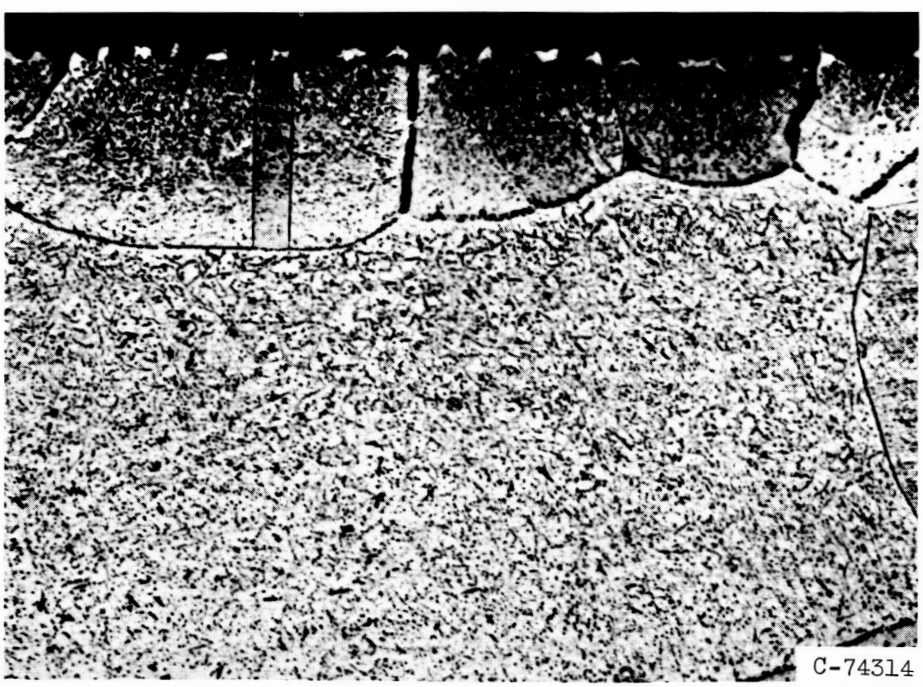

(c-2) As-oxidized plus stability heat treatment.

(c) Photomicrographs; magnesium content, 1.32 atomic percent. ×500.

Figure 6. - Continued. Micrographs of nickel-magnesium alloy oxidized for 200 hours at 1800° F before and after stability heat treatment. Marble's etch.

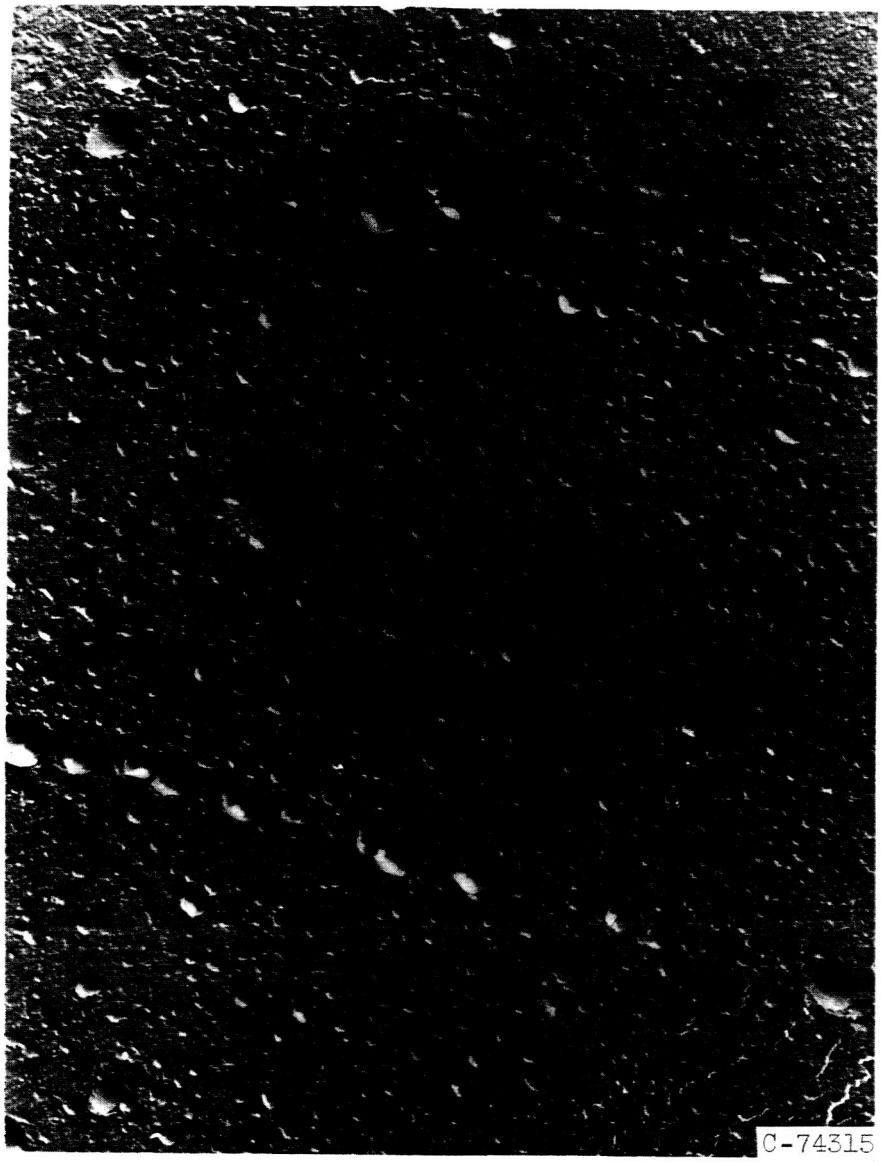

(d) Electron micrograph; magnesium content, 1.32 atomic percent; silicon monoxide replica. ×10 500.

Figure 6. - Concluded. Micrographs of nickel-magnesium alloy oxidized for 200 hours at 1800° F before and after stability heat treatment. Marble's etch.

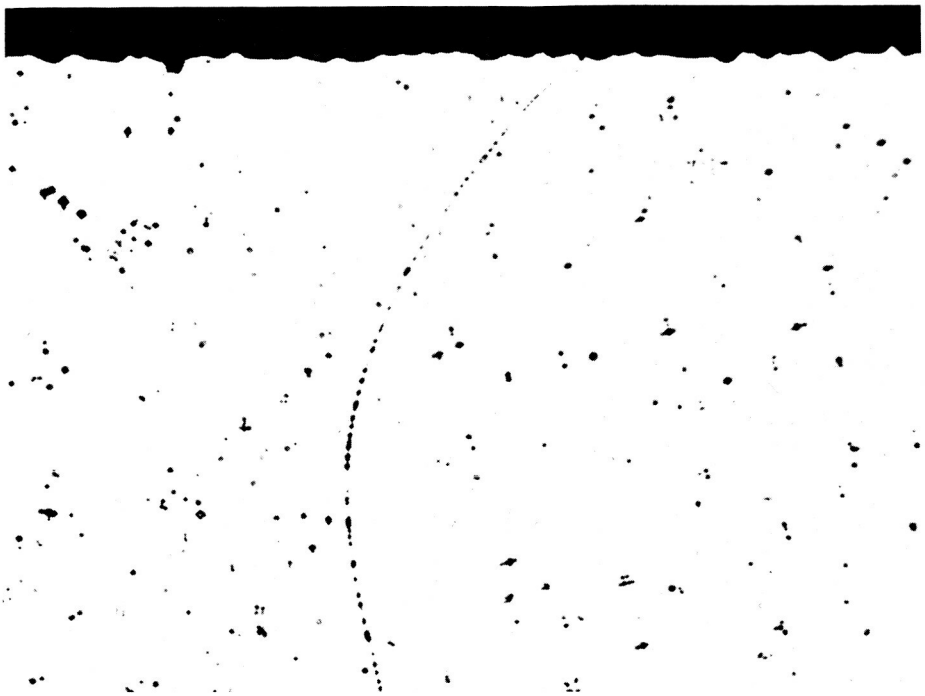

(a-1) As-oxidized.

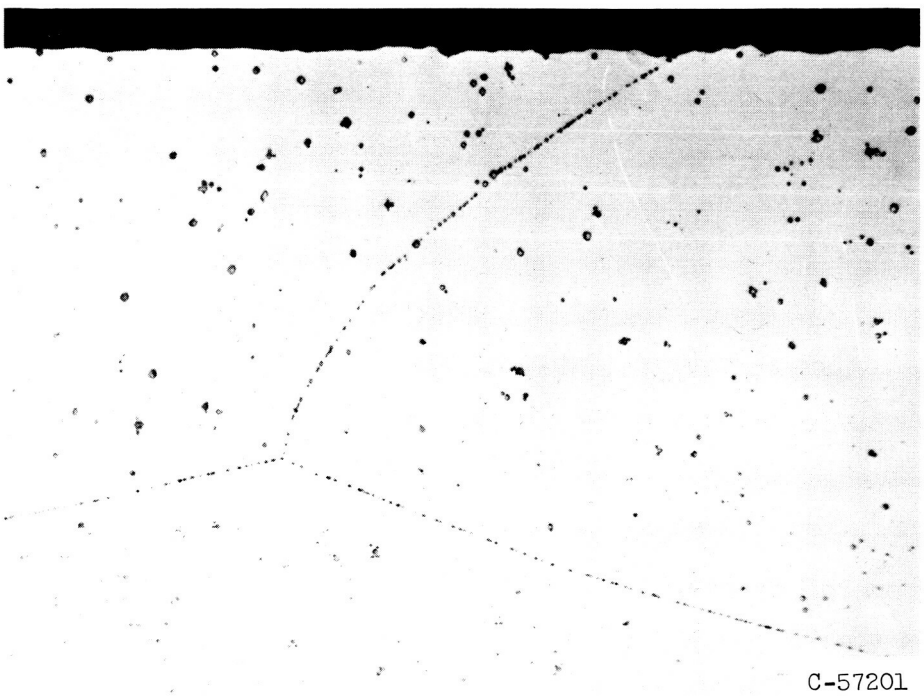

(a-2) As-oxidized plus stability heat treatment.

(a) Photomicrographs; silicon content, 0.073 atomic percent. ×500.

Figure 7. - Micrographs of nickel-silicon alloy oxidized for 200 hours at 1800° F before and after stability heat treatment. Marble's etch.

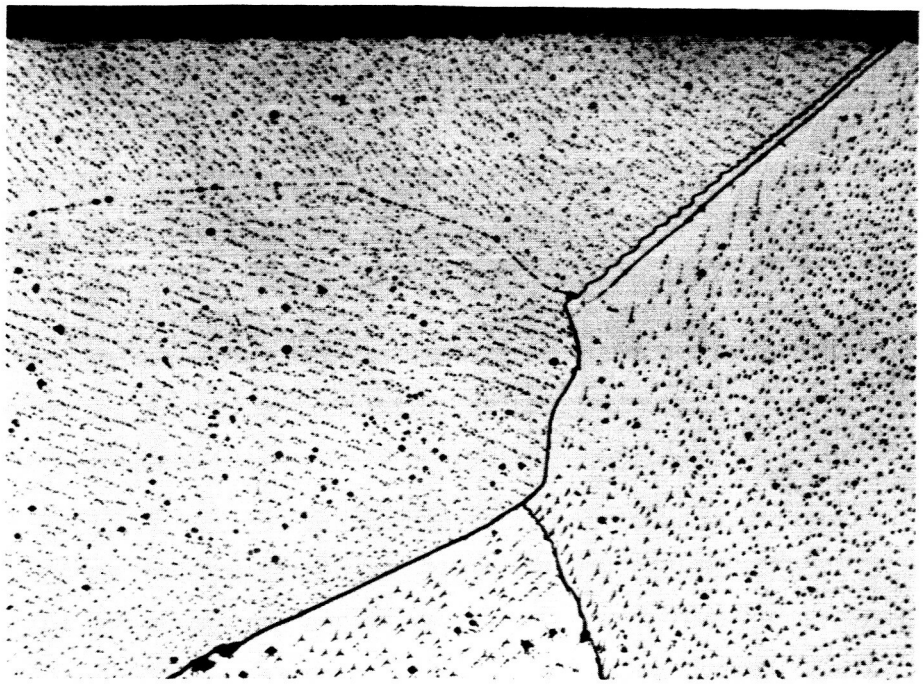

(b-1) As-oxidized.

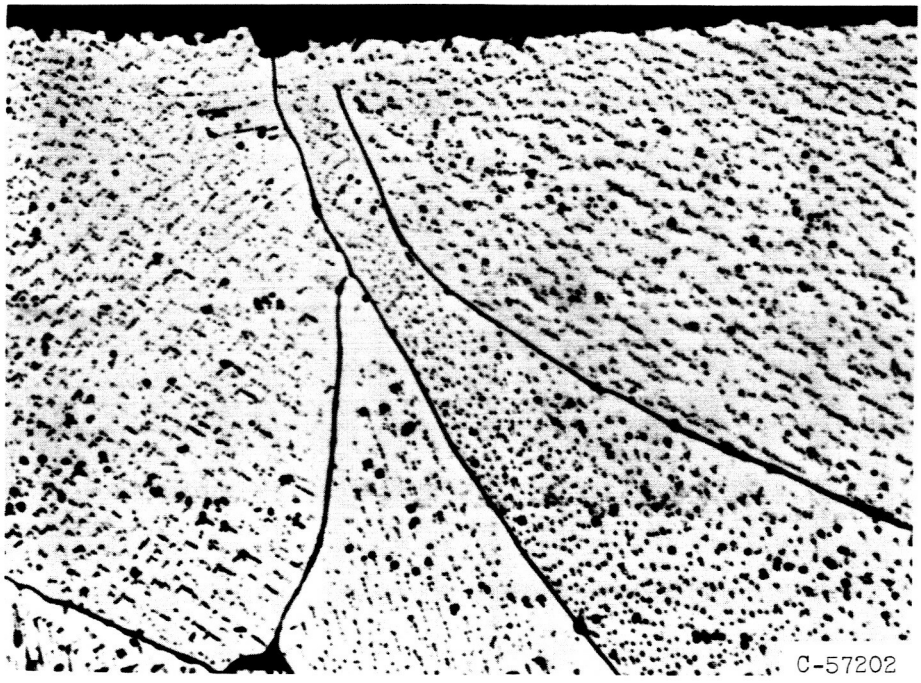

(b-2) As-oxidized plus stability heat treatment.

(b) Photomicrographs; silicon content, 0.98 atomic percent. ×500.

Figure 7. - Continued. Micrographs of nickel-silicon alloy oxidized for 200 hours at 1800° F before and after stability heat treatment. Marble's etch.

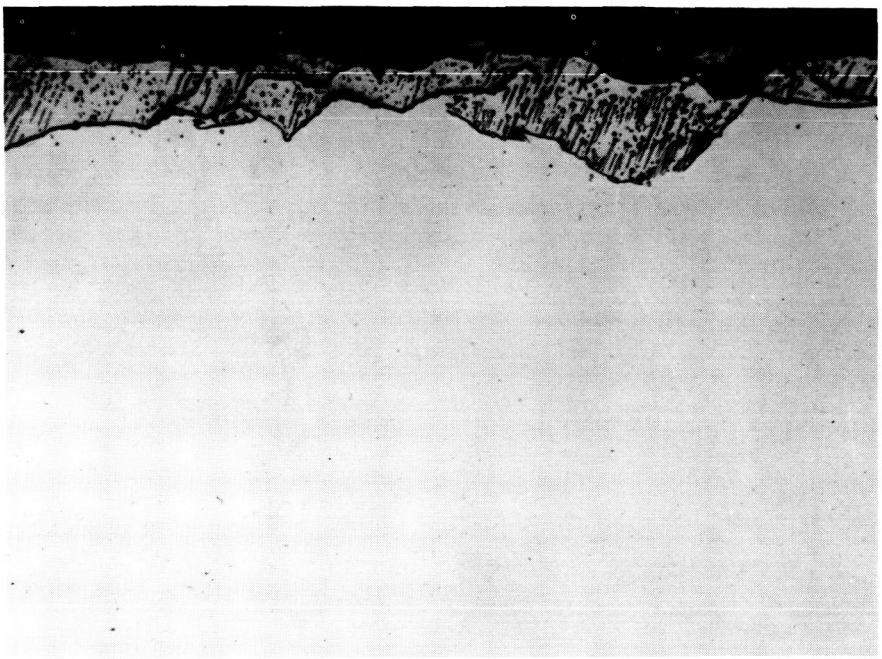

(c-1) As-oxidized.

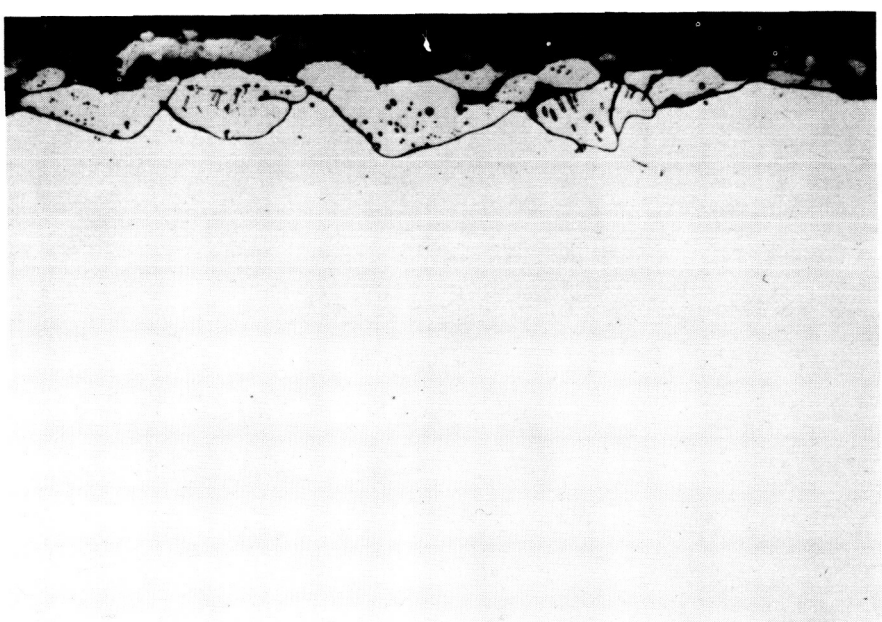

C-57101

(c-2) As-oxidized plus stability heat treatment.

(c) Photomicrographs; silicon content, 3.00 atomic percent. ×500.

Figure 7. - Continued. Micrographs of nickel-silicon alloy oxidized for 200 hours at 1800° F before and after stability heat treatment. Marble's etch.

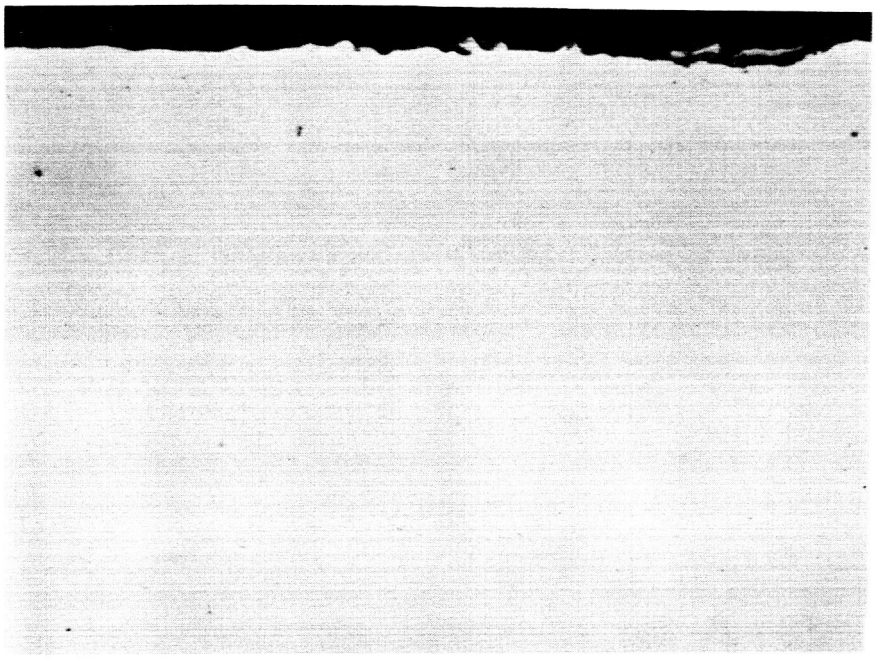

(d-1) As-oxidized.

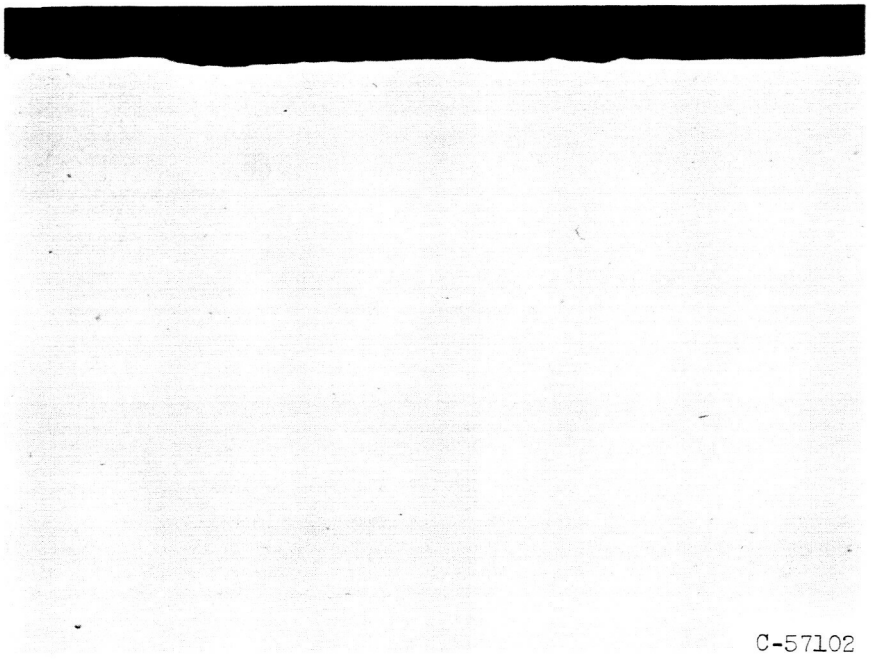

(d-2) As-oxidized plus stability heat treatment.

(d) Photomicrographs; silicon content, 8.77 atomic percent. ×500.

Figure 7. - Continued. Micrographs of nickel-silicon alloy oxidized for 200 hours at 1800° F before and after stability heat treatment. Marble's etch.

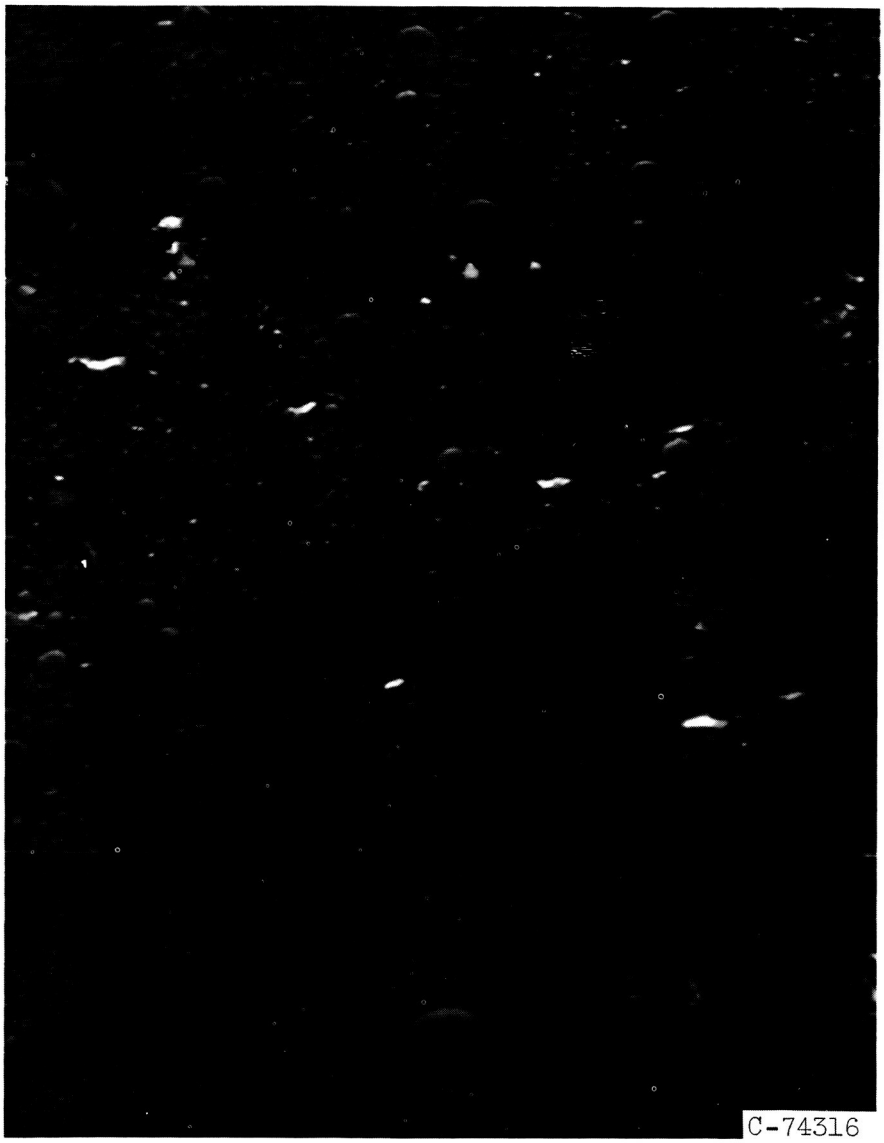

(e) Electron micrograph; silicon content, 0.98 atomic percent; silicon monoxide replica. ×9700.

Figure 7. - Concluded. Micrographs of nickel-silicon alloy oxidized for 200 hours at 1800° F before and after stability heat treatment. Marble's etch.

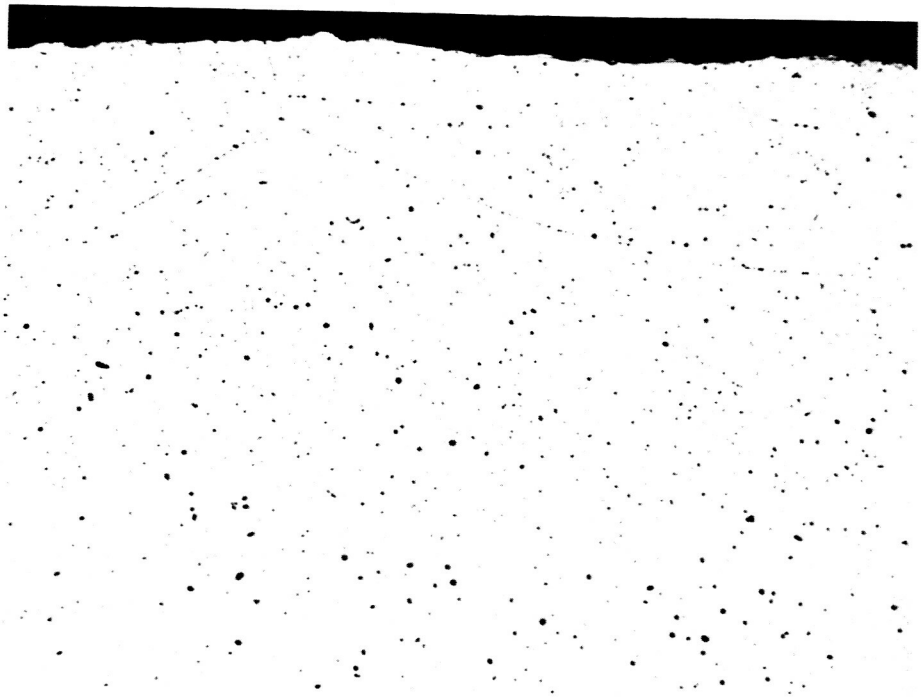

(a-1) As-oxidized.

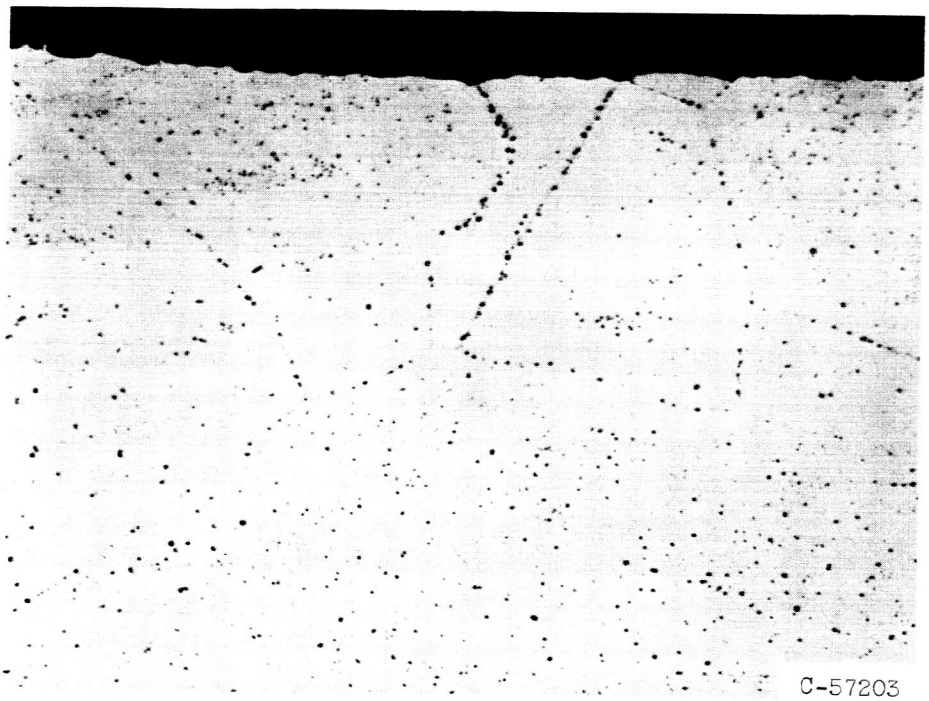

(a-2) As-oxidized plus stability heat treatment.

(a) Titanium content, 0.086 atomic percent.

Figure 8. - Photomicrographs of nickel-titanium alloy oxidized for 200 hours at 1800° F before and after stability heat treatment. Marble's etch. ×500.

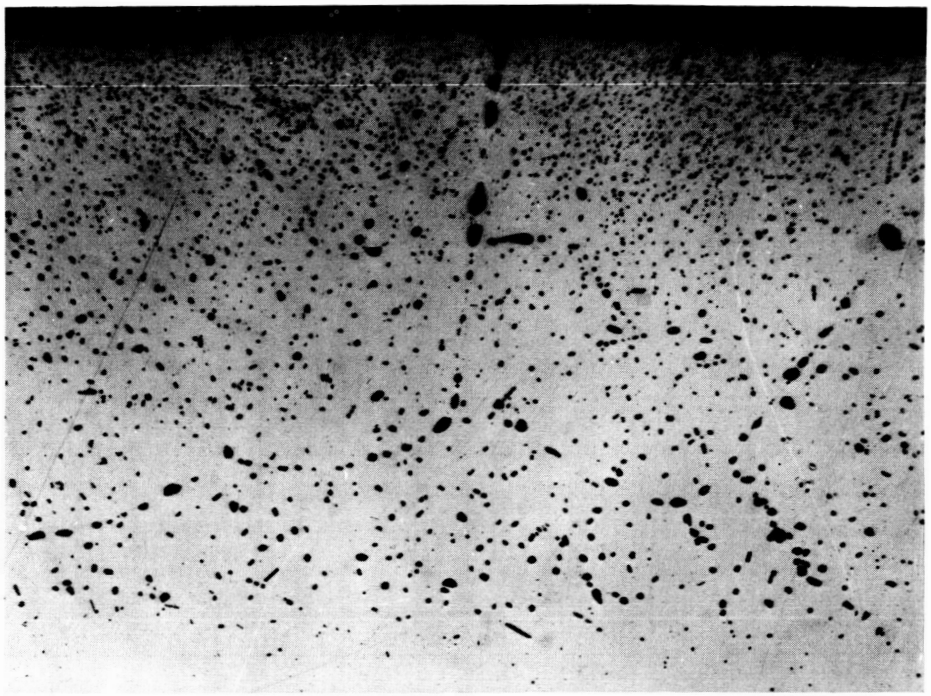

(b-1) As-oxidized.

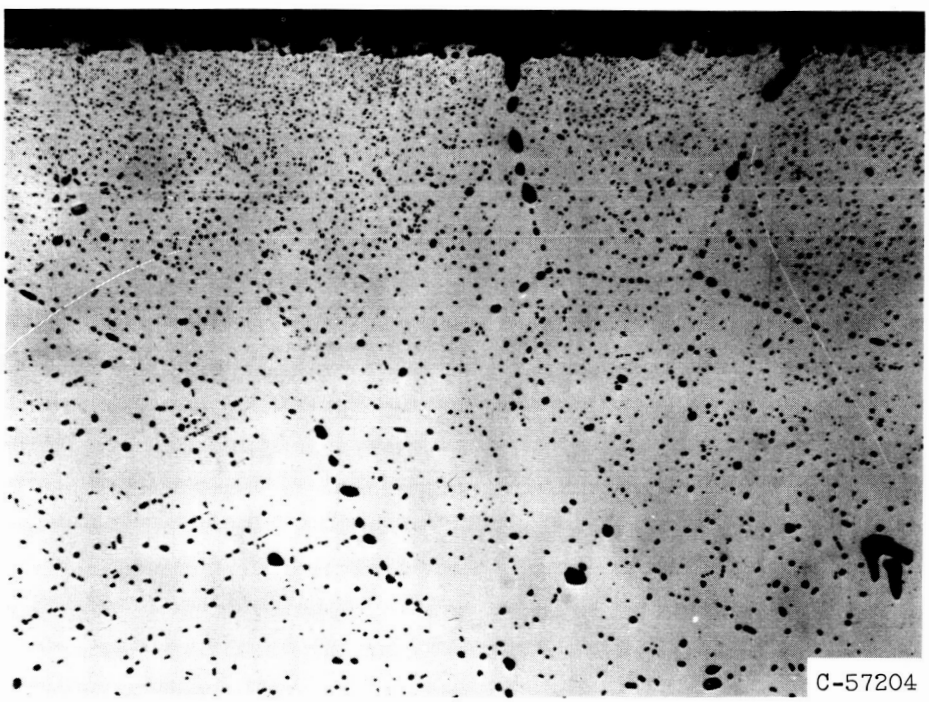

(b-2) As-oxidized plus stability heat treatment.

(b) Titanium content, 0.98 atomic percent.

Figure 8. - Continued. Photomicrographs of nickel-titanium alloy oxidized for 200 hours at 1800° F before and after stability heat treatment. Marble's etch. ×500.

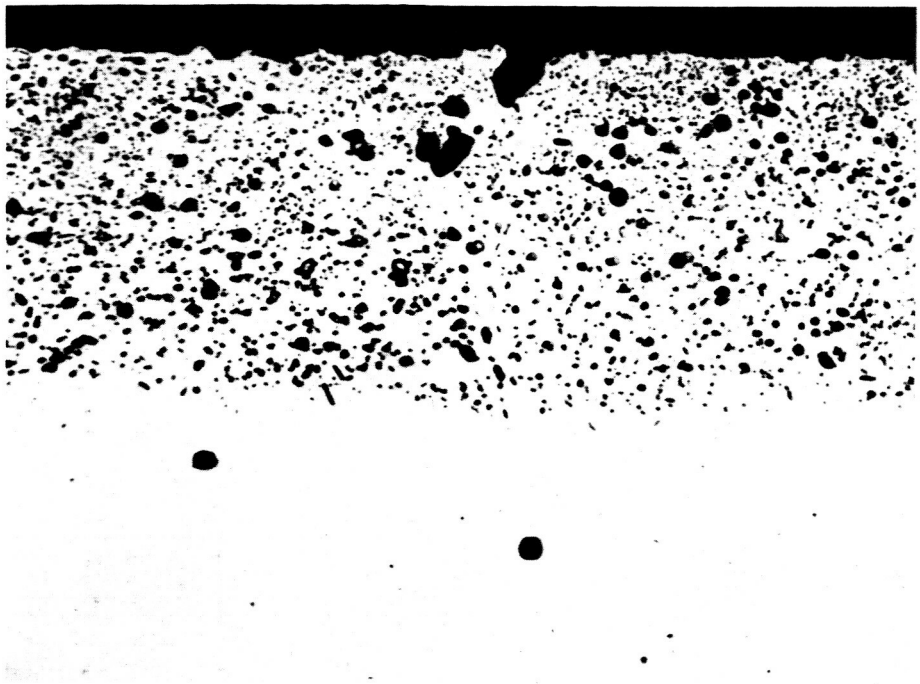

(c-1) As-oxidized.

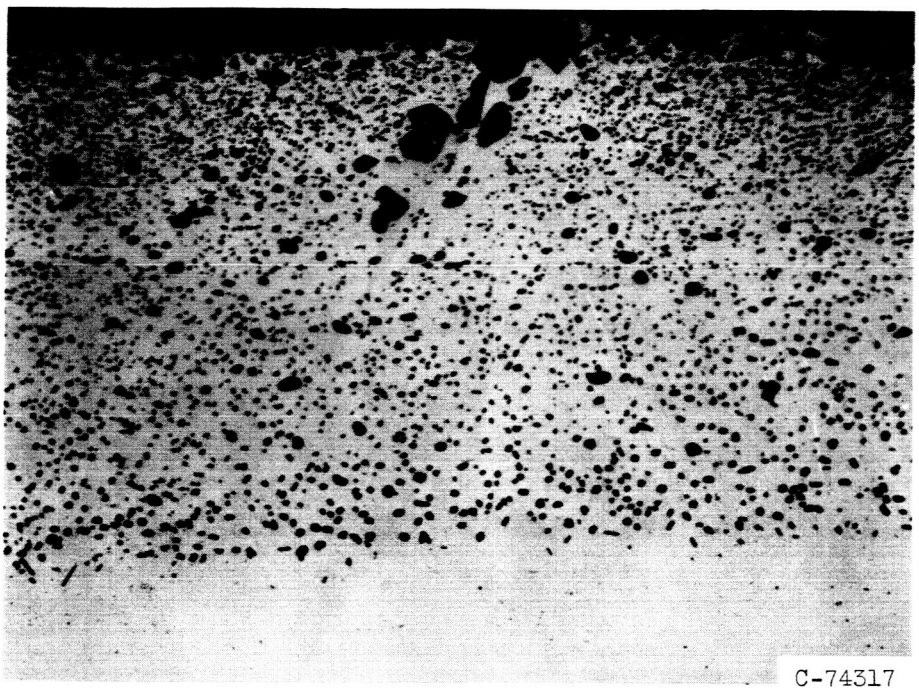

(c-2) As-oxidized plus stability heat treatment.

(c) Titanium content, 3.01 atomic percent.

Figure 8. - Continued. Photomicrographs of nickel-titanium alloy oxidized for 200 hours at 1800° F before and after stability heat treatment. Marble's etch. X500.

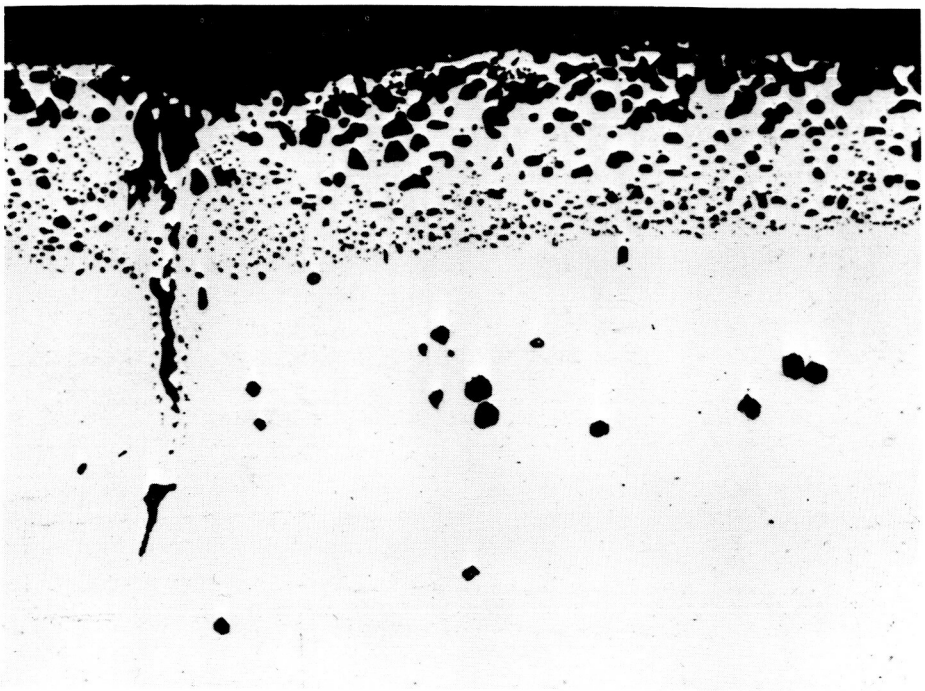

(d-1) As-oxidized.

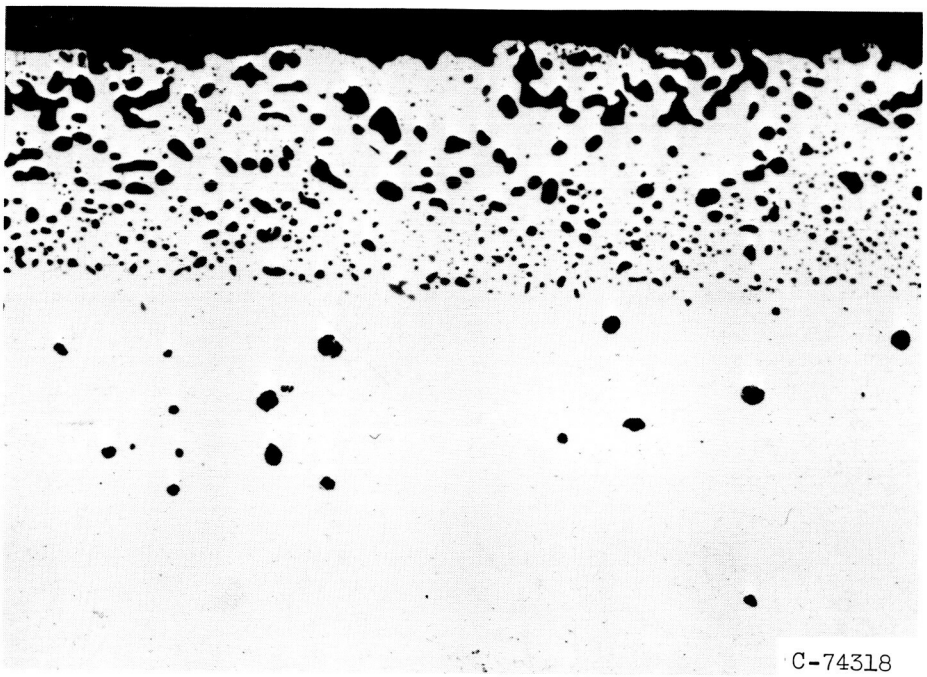

(d-2) As-oxidized plus stability heat treatment.

(d) Titanium content, 10.8 atomic percent.

Figure 8. - Concluded. Photomicrographs of nickel-titanium alloy oxidized for 200 hours at 1800° F before and after stability heat treatment. Marble's etch. ×500.

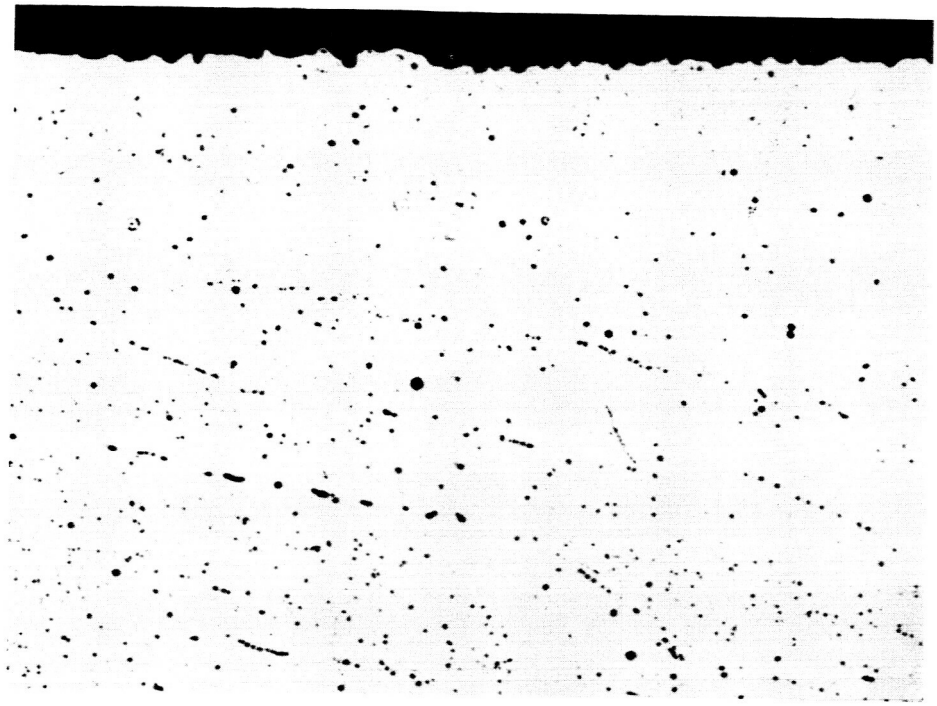

(a-1) As-oxidized.

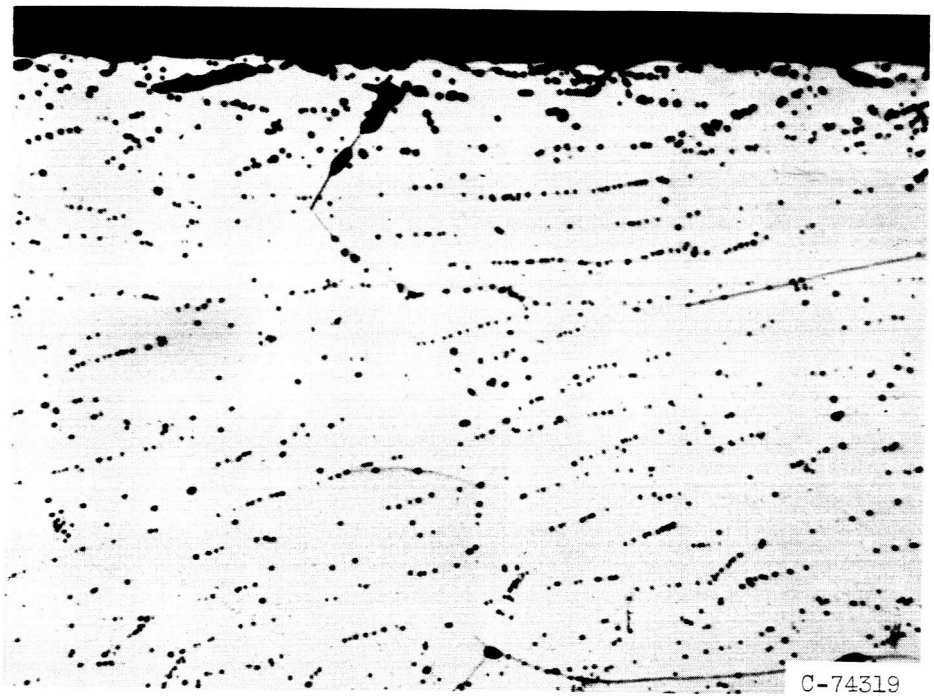

(a-2) As-oxidized plus stability heat treatment.

(a) Chromium content, 0.088 atomic percent.

Figure 9. - Photomicrographs of nickel-chromium alloy oxidized for 200 hours at 1800° F before and after stability heat treatment. Marble's etch. ×500.

(b-1) As-oxidized.

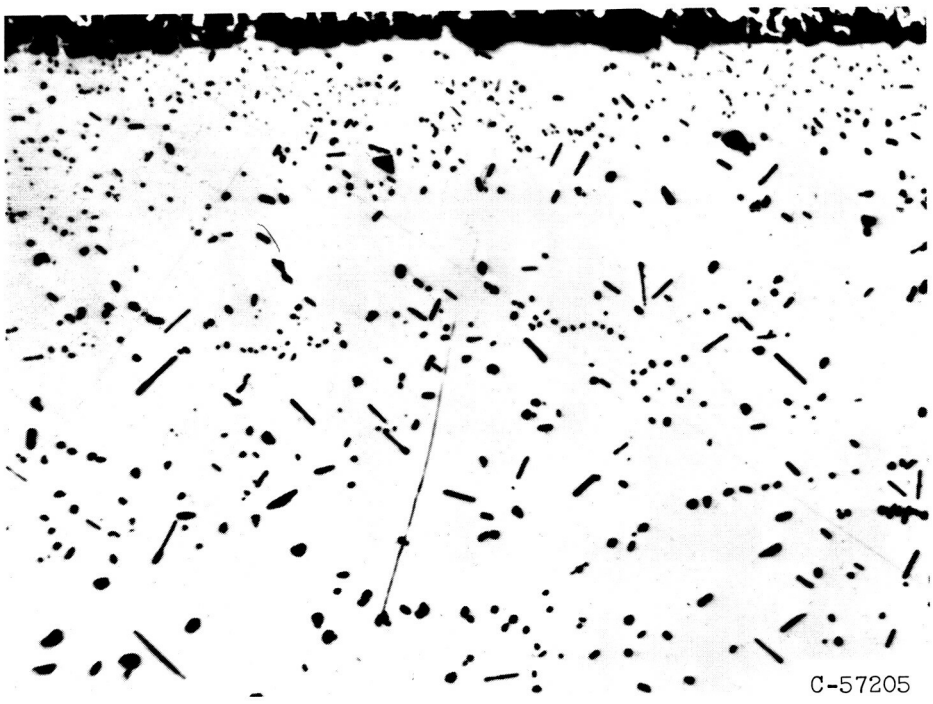

(b-2) As-oxidized plus stability heat treatment.

(b) Chromium content, 0.76 atomic percent.

Figure 9. - Continued. Photomicrographs of nickel-chromium alloy oxidized for 200 hours at 1800° F before and after stability heat treatment. Marble's etch. ×500.

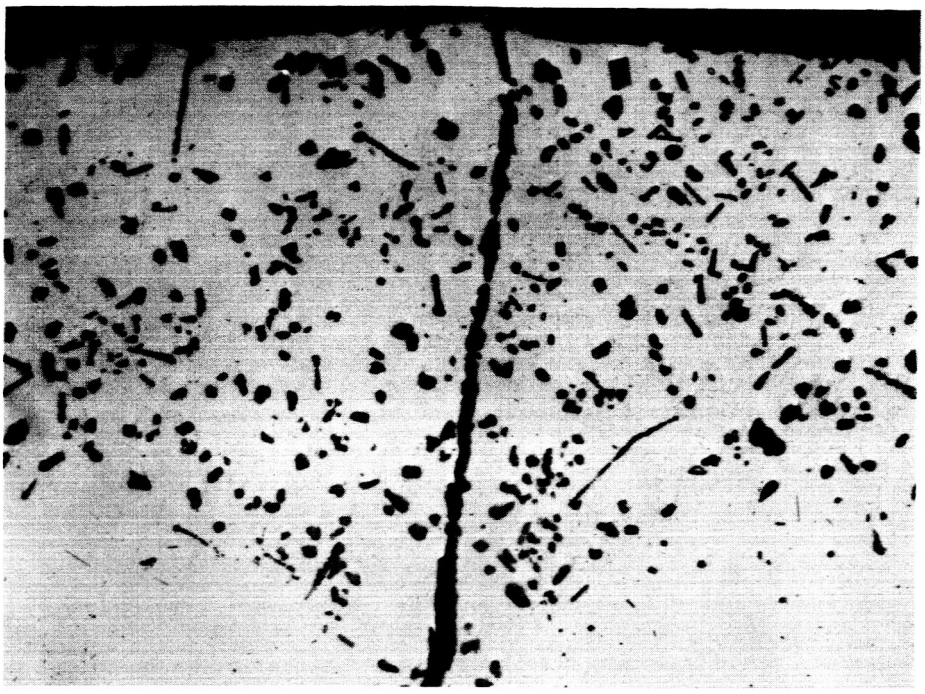

(c-1) As-oxidized.

C-74320

(c-2) As-oxidized plus stability heat treatment.

(c) Chromium content, 3.69 atomic percent.

Figure 9. - Continued. Photomicrographs of nickel-chromium alloy oxidized for 200 hours at 1800° F before and after stability heat treatment. Marble's etch. X500.

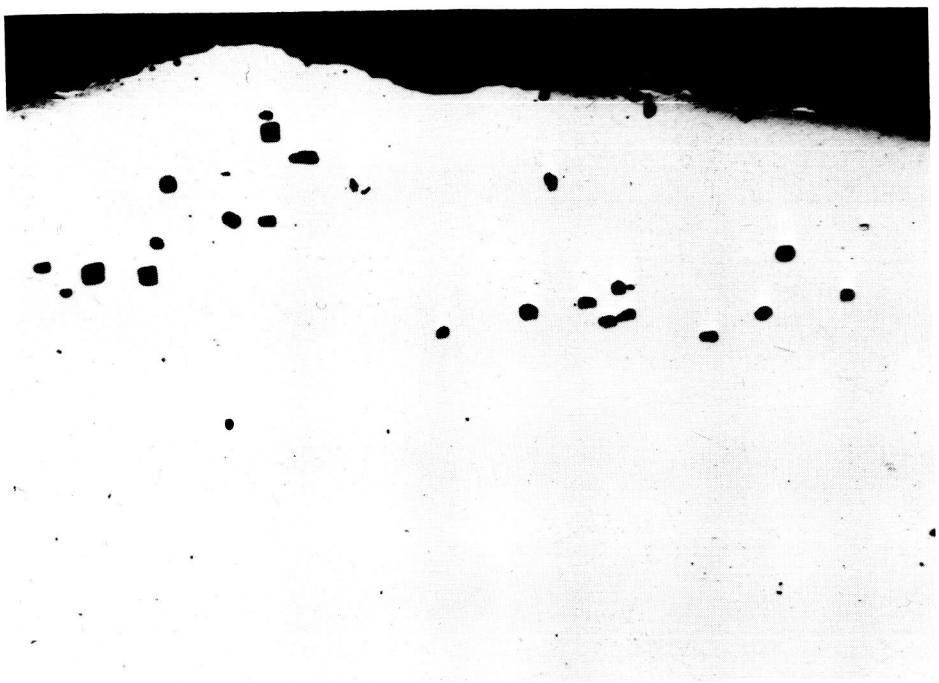

(d-1) As-oxidized.

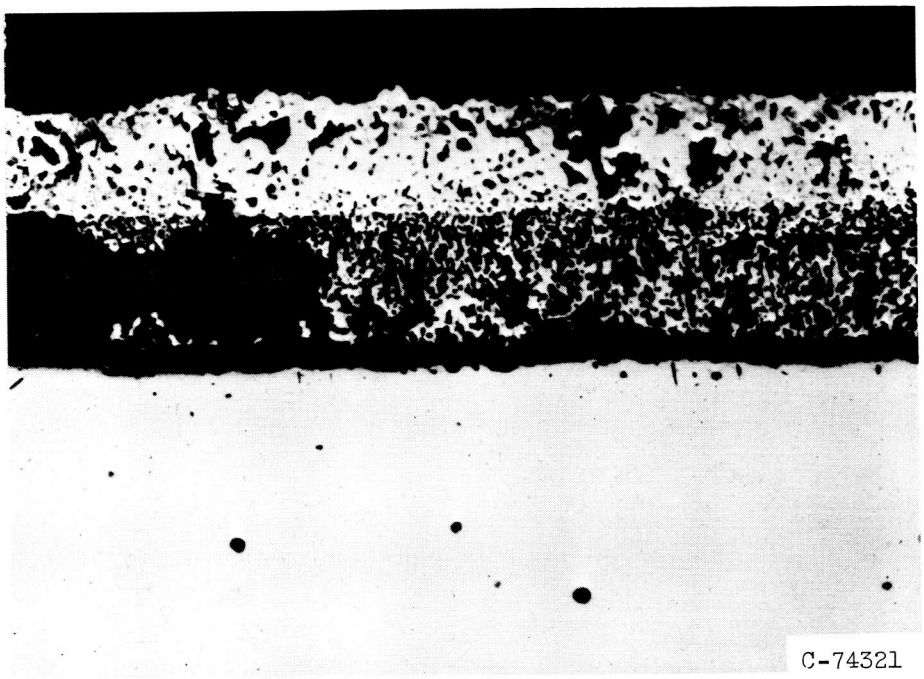

(d-2) As-oxidized plus stability heat treatment.

(d) Chromium content, 9.13 atomic percent.

Figure 9. - Concluded. Photomicrographs of nickel-chromium alloy oxidized for 200 hours at 1800° F before and after stability heat treatment. Marble's etch. ×500.

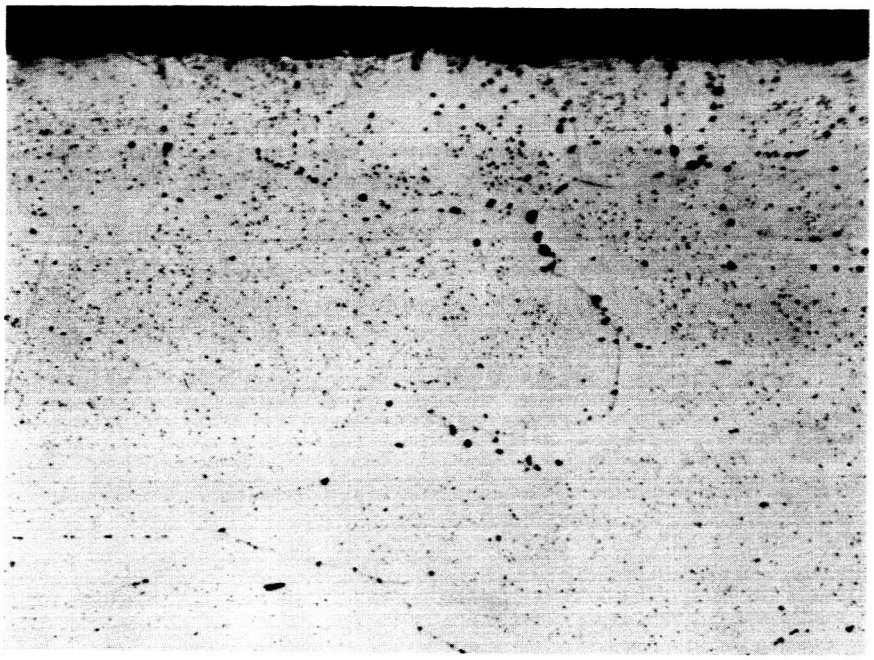

(a-1) As-oxidized.

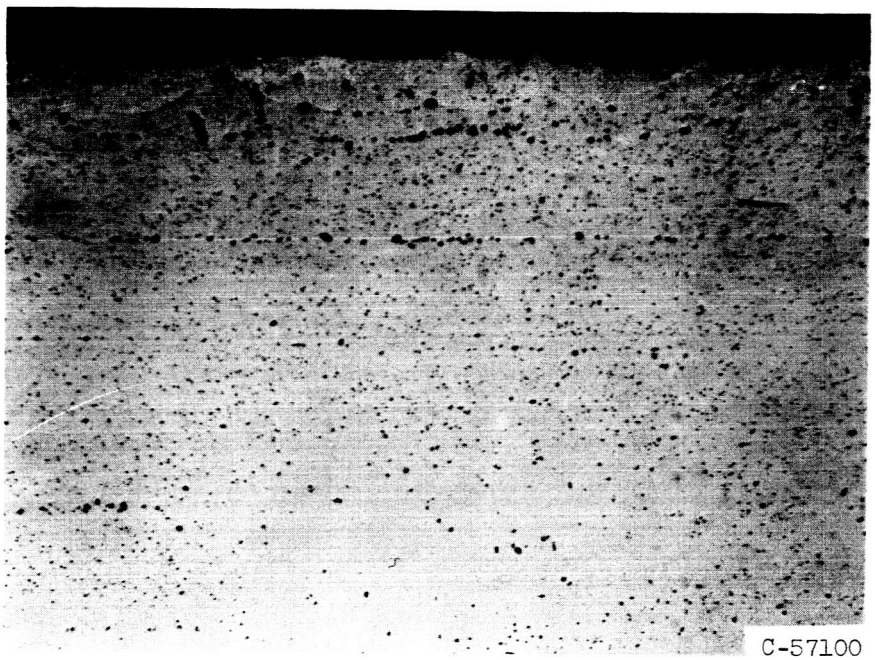

(a-2) As-oxidized plus stability heat treatment.

(a) Manganese content, 0.075 atomic percent.

Figure 10. - Photomicrographs of nickel-manganese alloy oxidized for 200 hours at 1800° F before and after stability heat treatment. Marble's etch. ×500.

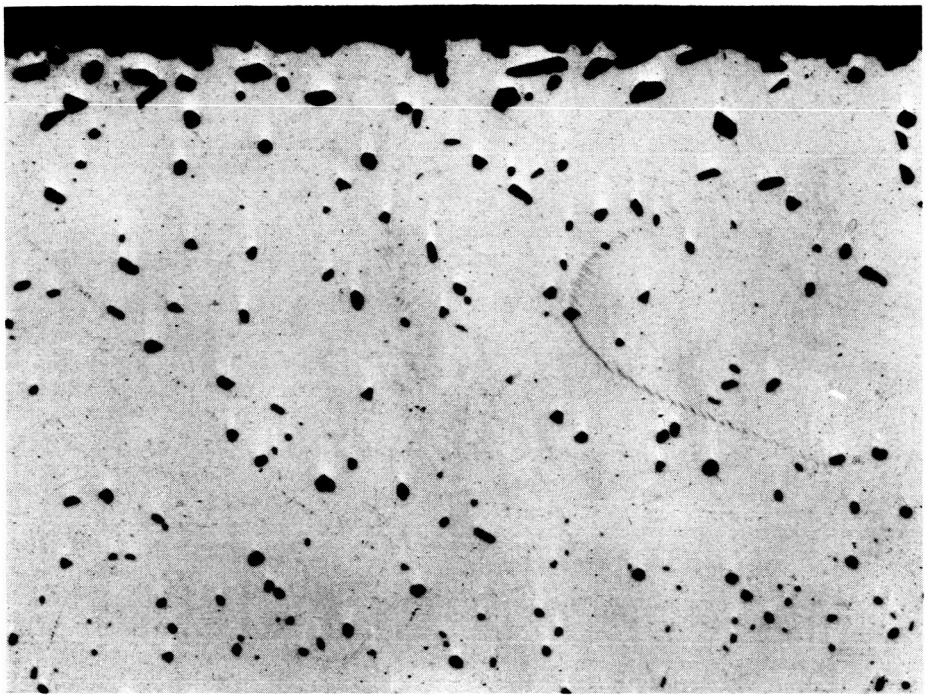

(b-1) As-oxidized.

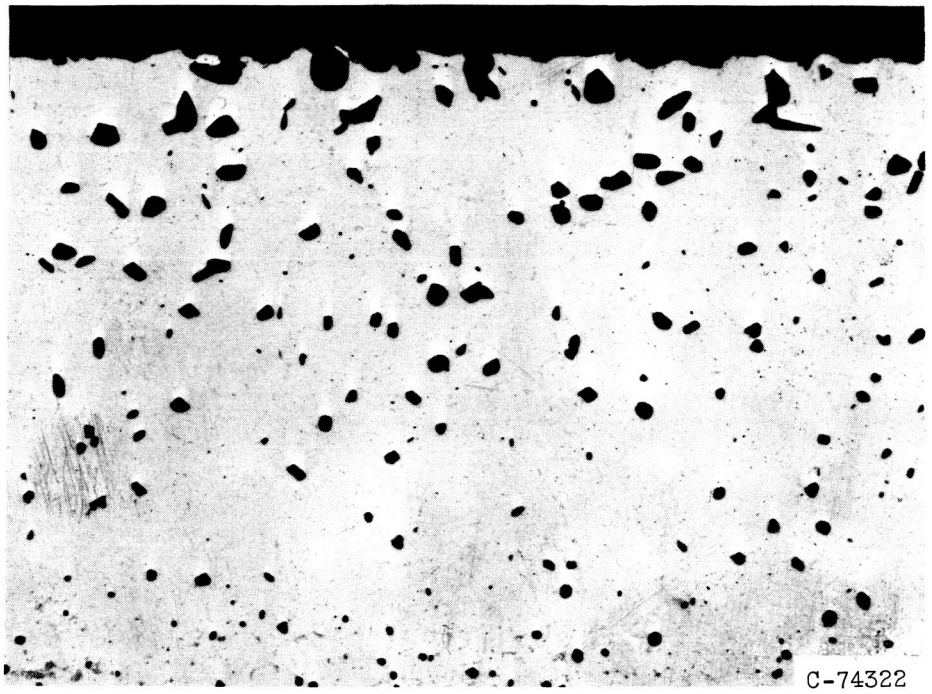

(b-2) As-oxidized plus stability heat treatment.

(b) Manganese content, 0.75 atomic percent.

Figure 10. - Continued. Photomicrographs of nickel-manganese alloy oxidized for 200 hours at 1800° F before and after stability heat treatment. Marble's etch. ×500.

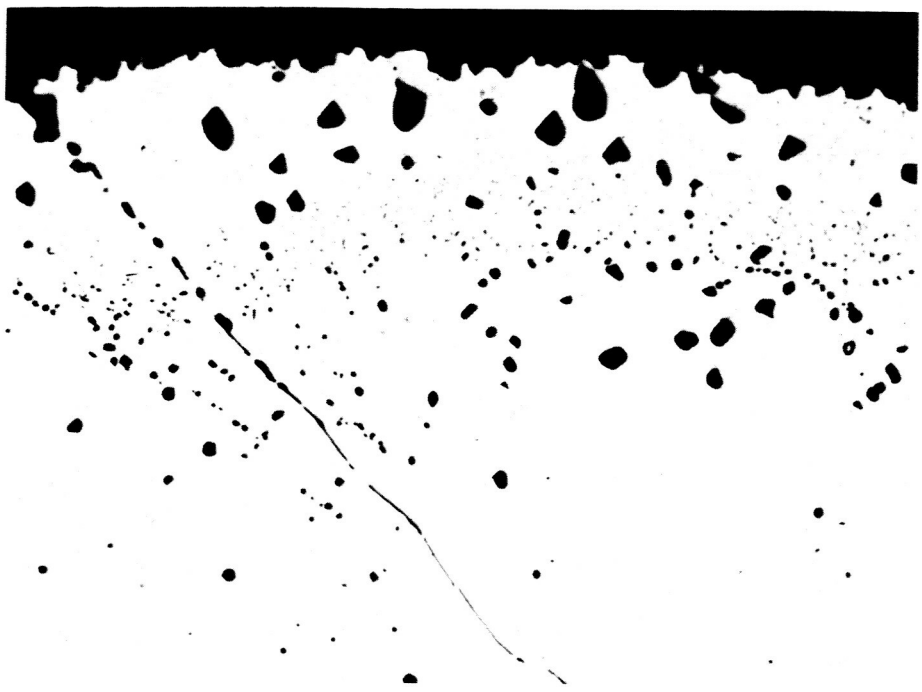

(c-1) As-oxidized.

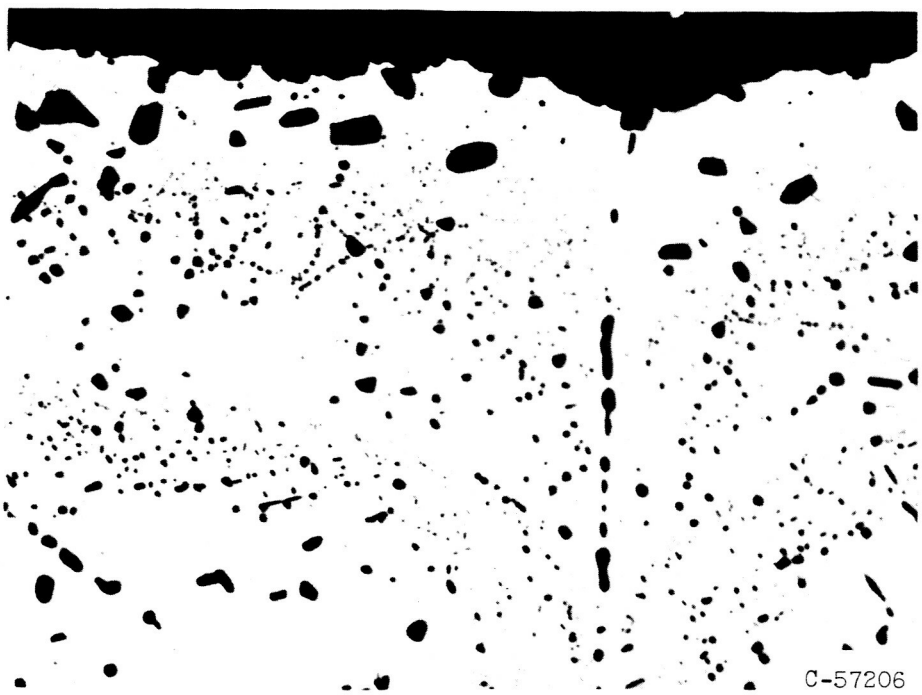

(c-2) As-oxidized plus stability heat treatment.

(c) Manganese content, 2.94 atomic percent.

Figure 10. - Continued. Photomicrographs of nickel-manganese alloy oxidized for 200 hours at 1800° F before and after stability heat treatment. Marble's etch. ×500.

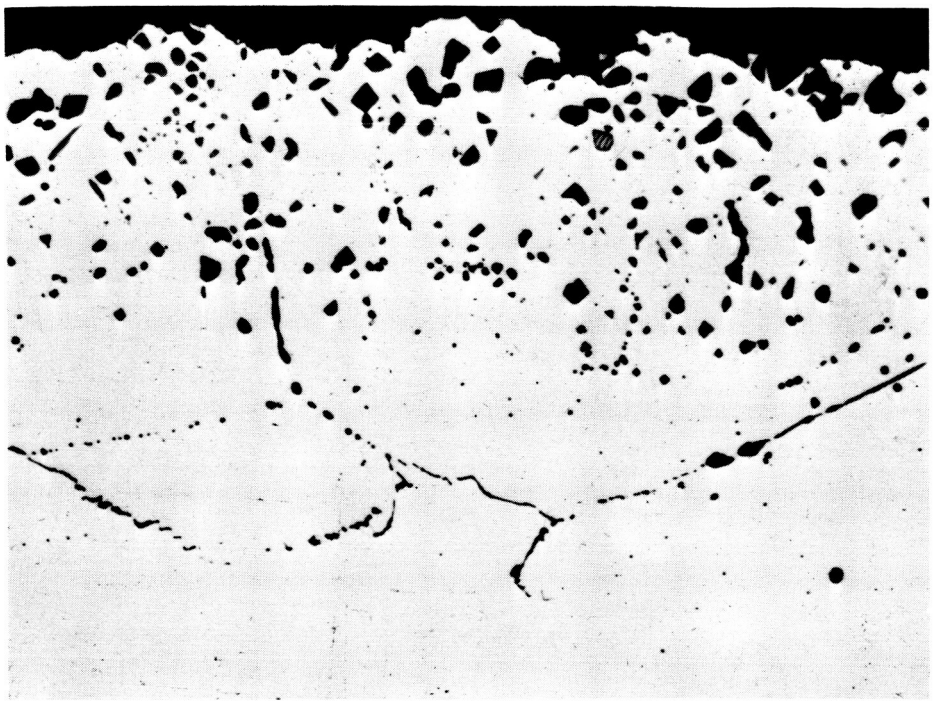

(d-1) As-oxidized.

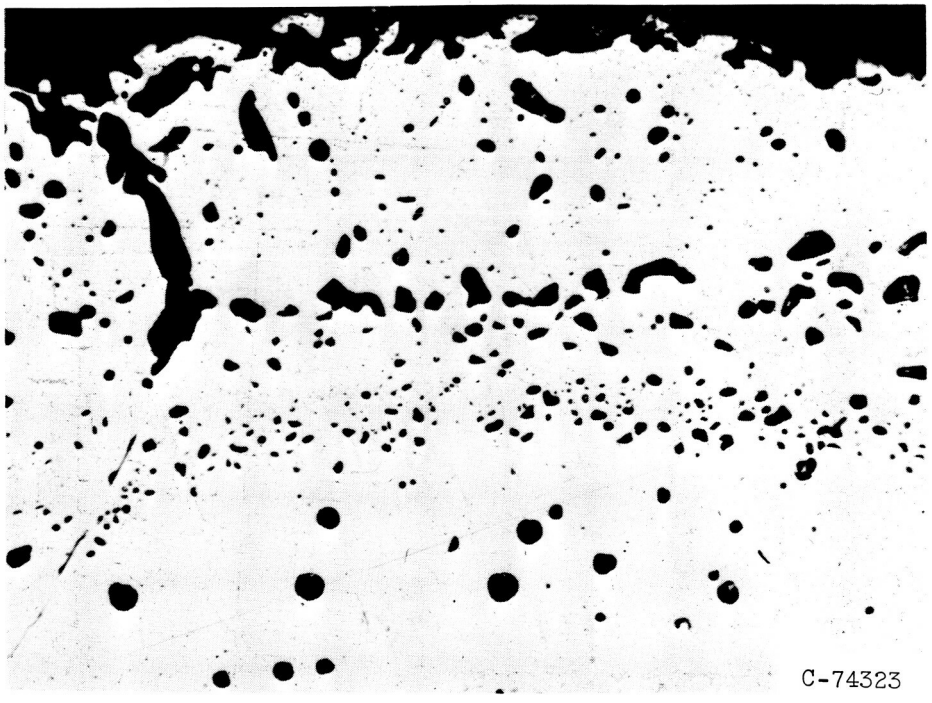

(d-2) As-oxidized plus stability heat treatment.

(d) Manganese content, 8.93 atomic percent.

Figure 10. - Concluded. Photomicrographs of nickel-manganese alloy oxidized for 200 hours at 1800° F before and after stability heat treatment. Marble's etch. X500.

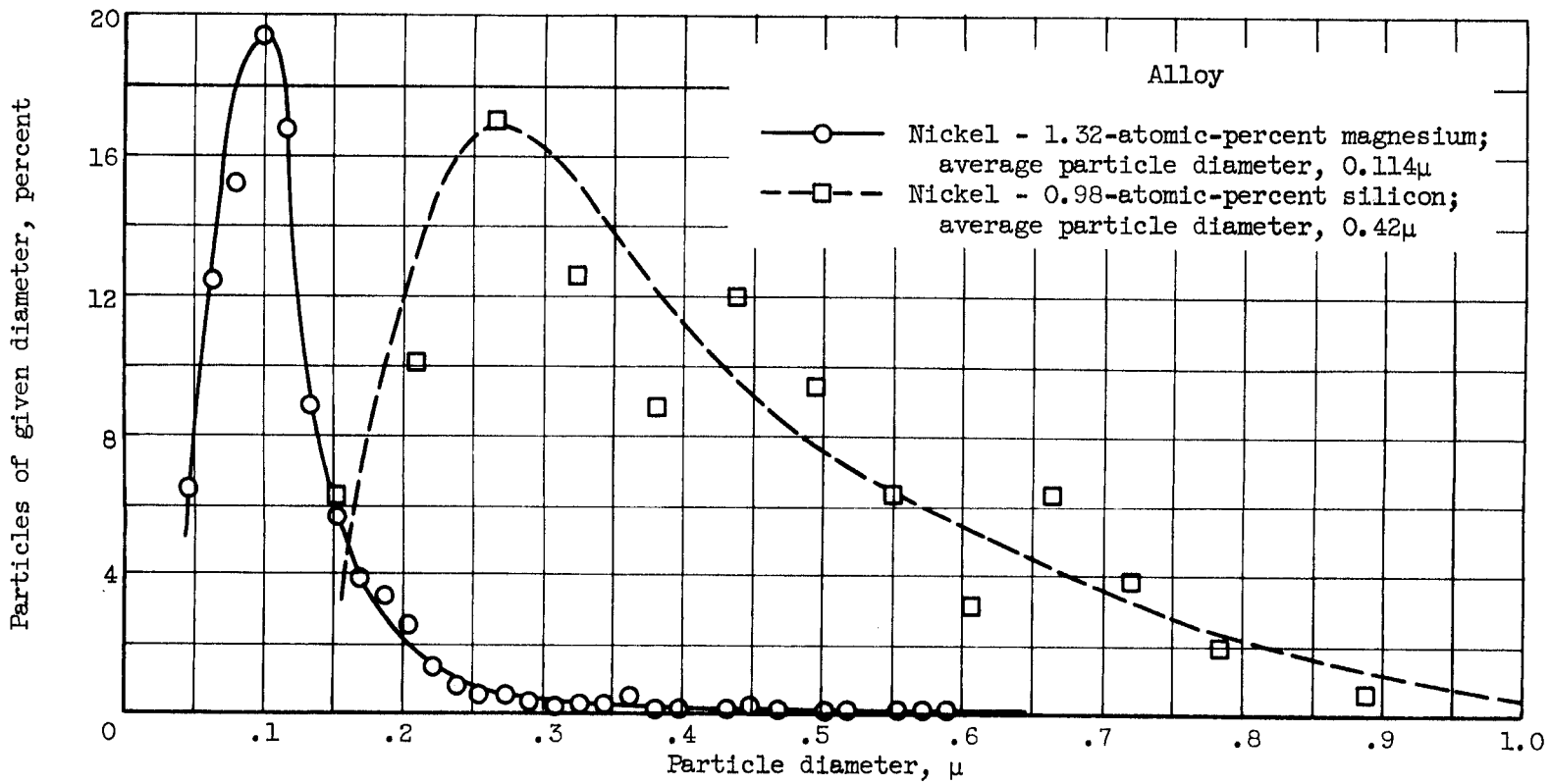

Figure 11. - Distribution of subscale oxide particle sizes developed in nickel - 1.32-atomic-percent magnesium and nickel - 0.98-atomic-percent silicon alloys after oxidation for 200 hours at 1800° F.

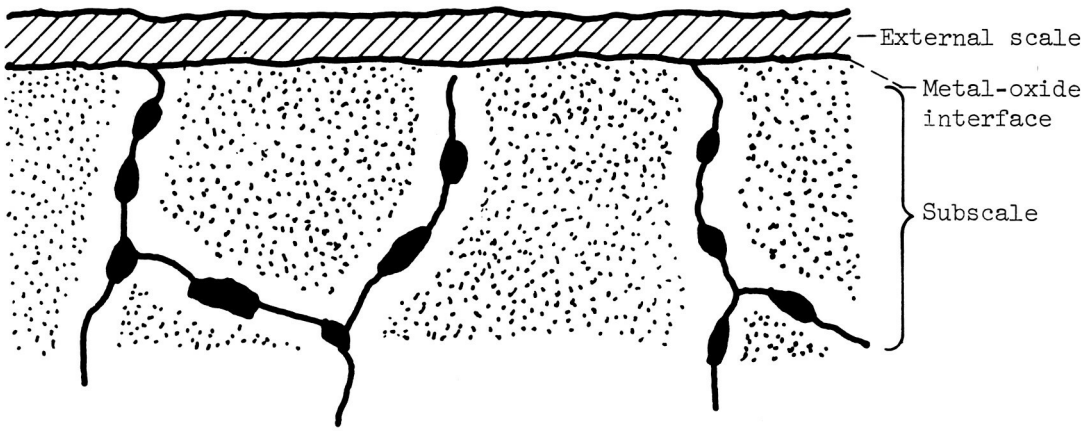

(a) Large oxides at grain boundaries relative to matrix oxides.

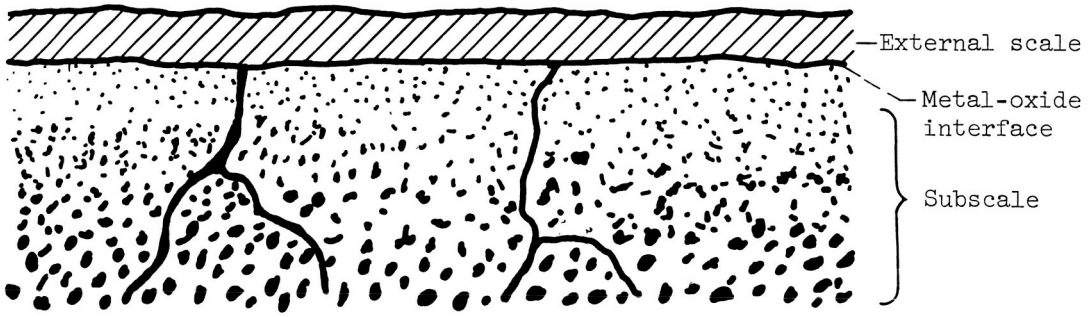

(b) Larger oxides at greatest penetrations.

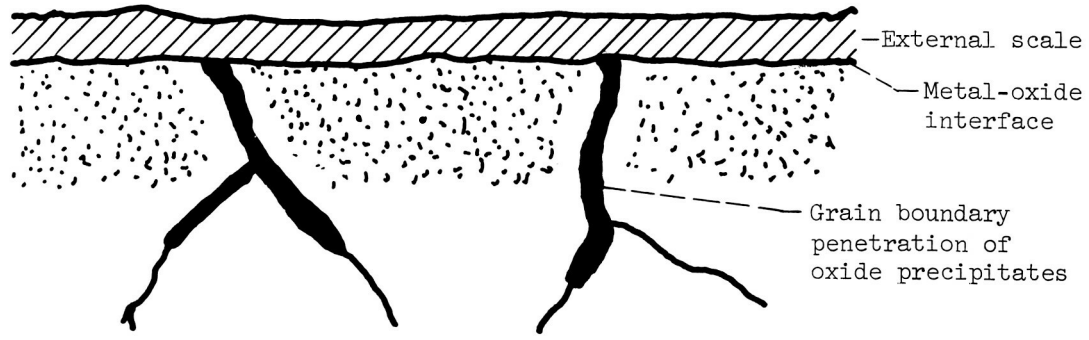

(c) Greater penetration rates in grain boundaries than in matrix.

Figure 12. - Schematics of undesirable microstructural configurations that can be produced by internal oxidation.